

# Annual Review of Condensed Matter Physics The Hubbard Model

## Daniel P. Arovas,<sup>1</sup> Erez Berg,<sup>2</sup> Steven A. Kivelson,<sup>3</sup> and Srinivas Raghu<sup>3,4</sup>

- <sup>1</sup>Department of Physics, University of California, San Diego, La Jolla, California, USA
- <sup>2</sup>Department of Condensed Matter Physics, Weizmann Institute of Science, Rehovot, Israel
- <sup>3</sup>Department of Physics, Stanford University, Stanford, California, USA; email: kivelson@stanford.edu
- <sup>4</sup>Stanford Institute for Materials and Energy Sciences, SLAC National Accelerator Laboratory and Stanford University, Menlo Park, California, USA



#### www.annualreviews.org

- Download figures
- · Navigate cited references
- · Keyword search
- · Explore related articles
- Share via email or social media

Annu. Rev. Condens. Matter Phys. 2022. 13:239-74

First published as a Review in Advance on November 18, 2021

The Annual Review of Condensed Matter Physics is online at commatphys.annualreviews.org

https://doi.org/10.1146/annurev-conmatphys-031620-102024

Copyright © 2022 by Annual Reviews. All rights reserved

#### Keywords

strongly correlated electrons, quantum materials, unconventional superconductivity, magnetism

#### Abstract

The repulsive Hubbard model has been immensely useful in understanding strongly correlated electron systems and serves as the paradigmatic model of the field. Despite its simplicity, it exhibits a strikingly rich phenomenology reminiscent of that observed in quantum materials. Nevertheless, much of its phase diagram remains controversial. Here, we review a subset of what is known about the Hubbard model based on exact results or controlled approximate solutions in various limits, for which there is a suitable small parameter. Our primary focus is on the ground state properties of the system on various lattices in two spatial dimensions, although both lower and higher dimensions are discussed as well. Finally, we highlight some of the important outstanding open questions.

#### 1. INTRODUCTION

The Hubbard model (1) has come to play a paradigmatic role in the theory of electronic correlations in quantum materials where interactions play an essential role. Its centrality in the quantum statistical mechanics of interacting fermions is comparable with that of the Ising model in classical statistical mechanics, yet almost sixty years after it was first described, there remain unsettled basic questions, even concerning the actual phases that arise for various lattice geometries. Conversely, the more progress that is made in obtaining theoretical solutions, the clearer it becomes that this simple model can exhibit a startling array of phases and regimes, many of which have clear parallels with observed behaviors of a wide variety of complex materials. For instance, there is compelling evidence that ferromagnetism, various forms of antiferromagnetism, unconventional superconductivity, charge-density waves (CDWs), electronic liquid crystalline phases, and topologically ordered phases (e.g., spin liquids), among other phases, occur in specific realizations of the Hubbard model.

It is our purpose here to summarize, to the extent possible in a brief article, what is established concerning the quantum phases of the Hubbard model. Although some discussion of the model on small clusters and in one dimension (d=1) is included for pedagogic purposes, the focus is primarily on the model on regular lattices (i.e., in the absence of disorder) in d=2 and d=3. Likewise, though we include some discussion of finite temperature results, our focus is on ground state properties, mostly to keep the scope of the article manageable. In the strong coupling limit and in the special case of one electron per site, the Hubbard model reduces to an insulating quantum Heisenberg antiferromagnet, which itself can exhibit many different and fascinating quantum phases; these are covered to an extent but mostly we focus on phases that occur for generic electron densities. Furthermore, we have mostly focused on equilibrium properties of the model, especially those essential thermodynamic correlation functions that characterize distinct quantum phases of matter.

Even within this limited scope, we have restricted ourselves to controlled solutions—by which we mean either exact results (typically obtained using numerical methods of various sorts) or cases in which there is an approximation scheme that becomes asymptotically exact as an explicitly identified small parameter tends to zero. This has led us to omit discussion of a variety of new and powerful mean-field methods, including dynamical mean-field theory and dynamical cluster approximations, which have profitably been applied to this problem. Fortunately, a companion paper to the present paper (2, also in this volume) has these approaches as its complementary focus.

We also do not explore the relation between the Hubbard model and experiments in any particular quantum material. Nonetheless, much of the modern resurgence of interest in this model is a consequence of the role it has played in the study of high-temperature superconductivity in the cuprates. Originally, this connection was suggested on rather basic phenomenological grounds (3, 4)—the parent state in the cuprates is a quasi-2D (two-dimensional) antiferromagnetic (AF) insulator, and the Hubbard model on the square lattice is the simplest possible model of a doped antiferromagnet. It is thus striking that many of the properties of this model that have been uncovered in subsequent theoretical studies resemble essential features of the electronic states of the cuprates that have been revealed by experiments, viz.: (a) The Hubbard model (at least for a range of U not too large) exhibits a dome of d-wave superconductivity throughout a range of doping. (b) It exhibits AF long-range order when undoped. (c) It evolves to an effectively weakly coupled Fermi liquid state upon heavy doping. (d) It exhibits a tendency toward formation of long-period unidirectional CDW and spin-density wave (SDW) orders (stripes) in the same range of doping in which superconducting correlations (at least locally) appear strongest. Indeed,

as in the materials themselves, the relation between density-wave and superconducting orders appears more complicated than the collocation competing orders might suggest, leading to their description as intertwined. As has been noted earlier (5), this congruence in behavior is sufficiently striking that it encourages the view that the solution of the Hubbard model can, in some sense, be considered to be the solution of the high  $T_{\rm c}$  problem.

#### 2. THEOREMS

The Hubbard model describes itinerant, interacting electrons of spin- $\frac{1}{2}$  hopping on a set  $\Lambda$  of spatially localized orbitals. The Hamiltonian is written as

$$\hat{H} = -\sum_{i,j\in\Lambda} \sum_{\sigma} t_{ij} c_{i\sigma}^{\dagger} c_{j\sigma} + U \sum_{i\in\Lambda} c_{i\uparrow}^{\dagger} c_{i\downarrow}^{\dagger} c_{i\downarrow} c_{i\uparrow},$$
1.

where the hopping  $t_{ij}$  is often restricted to nearest-neighbor sites, i.e.,  $t_{ij} = t_{ji}^* = t \, \delta_{|i-j|,1}$ , but generalizations can include further neighbor hopping and/or Peierls phase factors to account for nonzero magnetic flux. Unless explicitly noted, we confine our attention to the zero flux (time-reversal invariant) case. Furthermore, we consider only regular, connected lattices; i.e., we do not consider the effects of disorder. The electron filling is defined to be  $n \equiv N/|\Lambda|$  where  $|\Lambda|$  is the total number of sites and N is the number of electrons. The half-filled band, with one electron per site, corresponds to n = 1.

#### 2.1. Continuous Global Symmetries

The model's most apparent symmetry is a global U(2), under which  $c_{i\sigma} \to \mathcal{U}_{\sigma\sigma'} c_{i\sigma'}$  with  $\mathcal{U} \in \mathsf{U}(2)$  being the same matrix on all sites i. Separating  $\mathsf{U}(2) = \mathsf{U}(1) \times \mathsf{SU}(2)$ , the global U(1) invariance reflects global charge conservation, hence the total particle number  $\hat{N} = \sum_{i,\sigma} c_{i\sigma}^{\dagger} c_{i\sigma}$  is a good quantum number. This symmetry may be spontaneously broken in a superconducting state. The global  $\mathsf{SU}(2)$  invariance reflects spin isotropy, hence  $\hat{S}^z$  and  $\hat{S}^z$  are good quantum numbers, with  $\hat{S} = \frac{1}{2} \sum_{i,\mu,\nu} c_{i\mu}^{\dagger} \sigma_{\mu\nu} c_{i\nu}$ . Global  $\mathsf{SU}(2)$  invariance of the ground state is spontaneously broken in any ferromagnetic or AF state.

#### 2.2. Particle-Hole Symmetry

On a bipartite lattice, the transformation  $c_{i\sigma} \to \eta_i c_{i\sigma}^{\dagger}$ , where  $\eta_i = \pm$  on alternate sublattices, results in the transformed Hamiltonian,

$$\hat{H}' = -\sum_{i,j\in\Lambda} \sum_{\sigma} t_{ij} c_{i\sigma}^{\dagger} c_{j\sigma} + U \sum_{i\in\Lambda} c_{i\uparrow}^{\dagger} c_{i\downarrow} c_{i\downarrow} c_{i\uparrow} + U(|\Lambda| - \hat{N}).$$
 2.

At half-filling,  $\hat{N} = |\Lambda|$ , the model is particle–hole symmetric. In such cases, the system is proven (6) to be of uniform density, with  $\langle c_{i\sigma}^{\dagger} c_{j\sigma} \rangle = \frac{1}{2} \delta_{ij}$  if i and j are on the same sublattice (with no implicit sum on  $\sigma$ ). However, this does not preclude either magnetic or CDW order in the thermodynamic limit.

The SU(2) spin symmetry of the Hubbard model is generated by the operators,

$$\hat{S}^{+} = \sum_{i} c_{i\uparrow}^{\dagger} c_{i\downarrow}, \quad \hat{S}^{-} = (\hat{S}^{+})^{\dagger}, \quad \text{and} \quad \hat{S}^{z} = \frac{1}{2} \sum_{i} \left( c_{i\uparrow}^{\dagger} c_{i\uparrow} - c_{i\downarrow}^{\dagger} c_{i\downarrow} \right),$$
 3.

<sup>&</sup>lt;sup>1</sup>The conditions for uniform density from Reference 6 are much more general and include the possibility of site-dependent and even nonlocal interactions.

all of which commute with  $\hat{H}$  as well as with the number operator  $\hat{N} = \sum_{i,\sigma} c_{i\sigma}^{\dagger} c_{i\sigma}$ . A second, hidden SU(2) symmetry (7, 8) is present on bipartite lattices and is generated by the pseudospin operators,

$$\hat{J}^{+} = \sum_{i} \eta_{i} c_{i\uparrow}^{\dagger} c_{i\downarrow}^{\dagger}, \quad \hat{J}^{-} = (\hat{J}^{+})^{\dagger}, \quad \text{and} \quad \hat{J}^{z} = \frac{1}{2} (\hat{N} - |\Lambda|),$$

where  $\eta_i = \pm 1$  on the A and B sublattices, respectively. These operators also satisfy the SU(2) algebra  $[J^{\alpha}, J^{\beta}] = i\epsilon_{\alpha\beta\gamma}J^{\gamma}$ . Although the  $J^{\alpha}$ 's do not commute with  $\hat{H}$  and  $\hat{N}$  as do the generators  $S^{\alpha}$  for physical spin, they are eigenoperators in that

$$[\hat{K}, \hat{J}^{\pm}] = \pm (U - 2\mu)J^{\pm}$$
 5.

and  $[\hat{K}, \hat{J}^z] = 0$ , where  $\hat{K} = \hat{H} - \mu \hat{N}$  is the grand canonical Hamiltonian ( $\mu$  is the chemical potential). Thus, at half-filling, when  $\mu = \frac{1}{2}U$ , the Hubbard model has an additional SU(2) symmetry. Hence, the global symmetry group at half-filling is SO(4)  $\cong$  SU(2)  $\times$  SU(2)/ $\mathbb{Z}_2$ , where the  $\mathbb{Z}_2$  is associated with the fact that  $\hat{J}^z + \hat{S}^z$  has to be an integer when  $|\Lambda|$  is even and half-integer when  $|\Lambda|$  is odd (9).

#### 2.3. Lieb's Theorem

In 1989, Lieb (10) proved that for the attractive Hubbard model, with U < 0 (and allowing more generally for site-dependent  $U_i < 0 \ \forall i$ ), if the total number of electrons N is even, then the ground state of  $\hat{H}$  is unique and is a total spin singlet, i.e., with S = 0. A corollary is that if U > 0 (independent of i),  $\Lambda$  is bipartite with  $|\mathbf{A}| \geq |\mathbf{B}|$ , and  $N = |\Lambda|$  is even, then the ground state of  $\hat{H}$  has total spin  $S = \frac{1}{2}(|\mathbf{A}| - |\mathbf{B}|)$  and degeneracy 2S + 1 (i.e., spin degeneracy is the only degeneracy). A convenient example is the so-called Lieb lattice, in which the  $\mathbf{A}$  sublattice is a square lattice and there is a  $\mathbf{B}$  sublattice site at the center of every link (i.e., the  $\mathrm{CuO}_2$  lattice of the Emery model; 4). Lieb's proof extends the Perron–Frobenius argument deployed in one-dimensional (1D) systems (11) by invoking a tool known as spin-space reflection positivity. The theorem then entails a hierarchy of lowest energy levels in different total spin sectors,  $E_0(S) < E_0(S+1)$ , where  $S \in \{\frac{1}{2}(|\mathbf{A}| - |\mathbf{B}|), \dots, \frac{1}{2}|\Lambda| - 1\}$ . For bipartite lattices, the conditions of Lieb's theorem guarantee a ferromagnetic ground state when there is a sublattice imbalance, i.e.,  $|\mathbf{A}| \neq |\mathbf{B}|$ .

#### 2.4. Thouless-Nagaoka-Tasaki Theorem

An extension by Tasaki (12, 13) of the celebrated Nagaoka theorem (14), which in fact was originally proven in a more restricted form by Thouless (15), states the following: For the Hubbard model with  $U=\infty$  and arbitrary nonnegative  $t_{ij}$ , and with  $N=|\Lambda|-1$ , the ground state has total spin  $S=\frac{1}{2}N$  and degeneracy 2S+1. This establishes that there is a ferromagnetic ground state in the  $U\to\infty$  limit when the system is one electron shy of half-filling. No rigorous extension of these results to finite doped hole density has yet been achieved.

#### 2.5. The Lieb-Schultz-Mattis-Oshikawa-Hastings Theorem

The Lieb–Schultz–Mattis–Oshikawa–Hastings (LSMOH) theorem states, in essence, that "when the filling n is not an even integer, a unique, gapped, featureless, insulating ground state is impossible." It is useful to first consider the sort of behavior that is ruled out by the theorem but which may pertain if the conditions of the theorem are not met, examples of which are shown in **Table 1**. The Hubbard model in d = 1 is a band insulator when n = 0 or n = 2, but has a Mott phase for n = 1 that preserves all symmetries and with no adiabatic connection to a band

Table 1 Possible phases consistent with the LSMOH theorem

$n \notin 2\mathbb{Z}^a$	Uniqueb	Gapped	Featureless <sup>c</sup>	Insulator	<b>Example</b> <sup>d</sup>
✓	✓	✓	✓	✓	Not possible
<b>√</b>	<b>√</b>	Х	✓	Х	Metallic
<b>√</b>	<b>√</b>	✓	Х	✓	Density wave
<b>√</b>	✓	Х	✓	✓	Gapless spin liquid
<b>√</b>	Х	✓	✓	✓	Gapped spin liquid
Х	✓	✓	✓	✓	Band insulator

<sup>&</sup>lt;sup>a</sup>A checkmark in the first column indicates that the number of electrons per site is not an even integer.

Abbreviation: LSMOH, Lieb-Schultz-Mattis-Oshikawa-Hastings.

insulator. More generally, the theorem applies to models with any number of conserved flavors; in such a case, it states that a featureless, gapped ground state is impossible if the filling of at least one flavor per unit cell is a noninteger.

The original argument, due to Lieb, Schultz, and Mattis (LSM; 16), applied to an *N*-site, spin-*S XXZ* spin chain with periodic boundary conditions and zero total magnetization. LSM showed that if the ground state  $|\Psi_0\rangle$  is a state with crystal momentum  $K_0$ , i.e., if  $\hat{t} |\Psi_0\rangle = e^{iK_0} |\Psi_0\rangle$ , where  $\hat{t}$  is the lattice translation operator and we work in units where the lattice spacing is  $a \equiv 1$ , then the application of the spin twist operator,

$$\hat{V} = \exp\left(\frac{2\pi i}{N} \sum_{i=1}^{N} j \,\hat{S}_{j}^{z}\right),\tag{6}$$

results in a state  $|\Psi_1\rangle = \hat{V} |\Psi_0\rangle$  with crystal momentum  $K_1 = K_0 + 2\pi S$ , satisfying  $\langle \Psi_1 | \hat{H}_{XXZ} | \Psi_1 \rangle = E_0 + \mathcal{O}(1/N)$ . For exp  $(2\pi iS) = -1$ , the states are of different crystal momentum and, thus, orthogonal. Thus, in the thermodynamic limit any ground state  $|\Psi_0\rangle$  must be degenerate (or gapless). The theorem was extended to more general 1D systems in Reference 17.

Although the LSM argument does not apply in dimensions d>1, it was extended by Oshikawa (18) and subsequently rigorized by Hastings (19) to d-dimensional systems with periodic boundary conditions (i.e., on a d-torus) and a finite excitation gap. The line of reasoning, inspired by Laughlin's argument for quantization of the Hall conductivity in two dimensions (20), focuses on the consequences of adiabatic  $\phi=2\pi$  U(1) flux threading through one of the toroidal cycles, followed by a pullback to the original U(1) flux state. In the thermodynamic limit, starting with an initial ground state  $|\Psi_0(\phi=0)\rangle$ , this procedure results in a low-energy state  $|\Psi_1(\phi=0)\rangle$  (similar to the LSM construction), which becomes degenerate with the ground state in the thermodynamic limit. The analysis can be applied to bosonic systems as well (see, e.g., 21, 22).

#### 3. THE HUBBARD SQUARE AND ITS EXTENSIONS

The Hubbard square—that is, the four-site square molecule of Hubbard sites—is simple enough that its spectrum can be computed analytically (23), but already complicated enough that it hosts a variety of nontrivial many-body effects that shed considerable light on the more general problem (24). The symmetry (i.e., total spin S and transformation properties under the spatial symmetries of the square) of the ground state for the model with nearest-neighbor hopping, t, in different ranges of U/t and for different values of the electron number N between 0 and 4 is given

<sup>&</sup>lt;sup>b</sup>A checkmark in this column indicates whether a single, nondegenerate ground state on the torus is possible.

<sup>&</sup>lt;sup>c</sup>A checkmark in this column indicates that there is no spontaneous symmetry breaking of any kind (this does not exclude topological order).

<sup>&</sup>lt;sup>d</sup>The last column names a phase that is consistent with the listed properties, if any.

 $E_0$  for  $U \ll t$ N S Symmetry Range of U/t $E_0$  for  $U \gg t$ 0 0 any U 0 0 1 1 1/2 1 any U -2t-2t $-2\sqrt{2}t - 4t^2/U$  $-4t + U/4 - (5/128)U^2/t$ 0 2 any U 3 1/2  $U < U_{\text{Nag}}$  $-4t + U/2 - (7/128)U^2/t$ ND x, yND  $U_{\text{Nag}} < U$ 3/2 -2t

 $-4t + 3U/4t - (13/128)U^2/t$ 

 $-12t^{2}/U$ 

Table 2 Character of the ground state of the positive U Hubbard square

any U

Abbreviation: ND, no data.

 $(x^2 - y^2)$ 

in **Table 2**. In the absence of next-nearest-neighbor hopping, t' = 0, the model is particle–hole symmetric and the analogous results for  $4 < N \le 8$  are easily obtained.

The most remarkable feature of this table is that the ground state for N=4 and U>0 transforms nontrivially under spatial symmetries—it transforms according to the  $B_{1g}$  representation of the  $D_4$  spatial symmetries of the square (i.e., it transforms like  $x^2-y^2$ ). It is easy to prove (25) that no noninteracting model on the square can have this property; i.e., this is an intrinsically new effect of strong correlations. It is thus worthwhile to understand its origin.

It is possible to understand this property in the weak coupling limit. We start by considering the single-particle states for U=0. Treating the square as a four-site ring, all eigenstates may be labeled by a Bloch wave vector k. Provided |t'| < |t|, the single-particle states are ordered in energy such that the lowest (k=0) state has energy -2t-t', the next are the two-fold degenerate  $(k=\pm\pi/2)$  with energy +t' that transform as x and y, and the highest  $(k=\pi)$  state has energy 2t-t' and transforms as xy. Thus, for U=0, the ground state with N=4 is any state with two electrons (of opposite spin) in the k=0 state, and two electrons in either of the first excited states; it is thus six-fold degenerate. However, they can be expressed uniquely as states of given symmetry: There is a triplet of S=1 states that transform trivially under spatial transformations (rotations and mirror reflections), and three S=0 states, one (with one electron each in  $k=\pm\pi/2$ ) that transforms trivially under spatial transformations with two that are superpositions of states with two electrons either in  $k=\pi/2$  or  $k=-\pi/2$ , which transform either as xy or as  $x^2-y^2$ . Of these, the one that is adiabatically connected to the U>0 ground state is the latter,

$$\left|\Psi_{x^2-y^2}\right\rangle = \frac{1}{\sqrt{2}} \left[ c^{\dagger}_{\pi/2,\uparrow} c^{\dagger}_{\pi/2,\downarrow} - c^{\dagger}_{-\pi/2,\uparrow} c^{\dagger}_{-\pi/2,\downarrow} \right] c^{\dagger}_{0\uparrow} c^{\dagger}_{0\downarrow} \left| 0 \right\rangle. \tag{7}$$

Given that there are no degeneracies once symmetry is imposed, it is clearly possible to incorporate the effects of small U by straightforward perturbation theory. Hund's first rule, which in this context would be expected to be derivable in first-order perturbation theory, would imply that the triplet state would be the most likely candidate ground state. Indeed, for any Slater determinant state, the first-order energy is  $4UN_{\uparrow}N_{\downarrow}$ , where  $N_{\sigma}$  is the number of electrons with given spin polarization, and this takes its minimal value of 3U/4 in a triplet state with three electrons of one polarization and one electron of the opposite polarization. However, manifestly  $|\Psi_{x^2-y^2}\rangle$  is not a Slater determinant, and indeed it is easy to show that, to first order in U, it is degenerate with the triplet state. Computing the second-order correction requires a bit of algebra, but the result (given for t'=0 in **Table 2**) is that the singlet state has the lower energy.

This is a rare example of a case in which Hund's rule is violated. Note that the cause of this is a subtle quantum effect—the ground state in the  $U \rightarrow 0$  limit is a highly entangled state that does not reduce to a single Slater determinant.

The other case that has interesting structure is the N=3 square. For U=0, the ground state is four-fold degenerate, but this degeneracy is fixed by symmetry and, hence, survives to nonzero U. Specifically, the ground state has S=1/2 and  $k=\pm\pi/2$ ; i.e., it transforms under the spatial symmetries as (x,y). However, for large U, we know from Nagaoka's theorem that the ground state must have S=3/2. Because parallel spins do not interact in the Hubbard model, this state is the noninteracting (Slater determinant) state with one electron in each of k=0 and  $\pm\pi/2$ ; the resulting state is manifestly invariant under the spatial symmetries. It requires a little algebra to derive the critical value of  $U=U_{\rm Nag}$  that separates the two regimes; for t'=0,  $U_{\rm Nag}=4(2+\sqrt{7})$   $t\approx 18.6t$ .

It is also interesting to consider an ensemble of Hubbard squares. If they can exchange particles, we can ask the following question: If we have a total of N electrons (with  $0 < N \le 8$ ) and two molecular Hubbard squares on which to place them, what is the lowest energy state? Not surprisingly, for N=8 it is best to put four electrons on each molecule, whereas for N=7 it is best to place three on one molecule and four on the other. However, for N=6, the result is more interesting. We define the pair binding energy,

$$\Delta_{\rm p} \equiv 2 E(3) - E(4) - E(2),$$
 8.

where E(n) is the n-electron ground state energy of a molecule.  $\Delta_p$  is the energy difference between placing three electrons (one doped hole) on each molecule, or two electrons (one pair of doped holes) on one and four electrons (no holes) on the other.  $\Delta_p$  is negative for U larger than a certain value  $U_p$ , as one might have expected, but it is positive for  $U < U_p$ ; i.e., there is an effective induced attraction between two doped holes. (For t' = 0,  $U_p \approx 4.584t$ .)

The existence of a range of U>0 in which  $\Delta_{\rm p}>0$  constitutes the simplest paradigmatic example of a system in which an effective attraction—indeed induced pairing—arises from purely repulsive microscopic interactions. Ultimately, it is related to the anomalous stability of the state with four electrons on one molecule. In the weak coupling limit, the pair binding can be computed perturbatively as  $\Delta_{\rm p}=A\,U^2/t+\dots$ , where A is a function of t'/t with A=1/32 for t'=0. One can also consider the separate contributions of the kinetic energy (hopping term) and the interaction energy (Hubbard term) to  $\Delta_{\rm p}$ . In the weak coupling limit, pair formation is associated with a cost in kinetic energy that is more than compensated by a reduced cost in repulsion, but for  $U_{\rm p}>U>U^*$  (where  $U^*\approx 2.457\,t$  for t'=0),  $\Delta_{\rm p}$  gets a positive contribution from a lowering of the kinetic energy and a negative contribution (disfavoring pair binding) from the interactions. An intrinsically strong coupling mechanism of "kinetic-energy driven pairing" is thus in play for  $U^*< U< U_{\rm p}$ .

One final lesson from this concerns the preferred symmetry of a pairing order parameter. Consider the operator  $\hat{\Phi} = \sum_{i,j} \phi_{i,j} \, c_{i\uparrow} \, c_{j\downarrow}$  that creates the two-electron ground state by acting on the undoped (four electron) ground state. This operator can be viewed as creating a Cooper pair of doped holes. As first observed by Scalapino & Trugman (24), the symmetry properties of  $\hat{\Phi}$  are determined by the *difference* of the spatial symmetries of two and four electron ground states. For the case tabulated above valid for |t'| < |t|, this means that this operator has  $d_{x^2-y^2}$  symmetry. This illustrates the robust preference for d-wave superconductivity that is a generic feature of the Hubbard model on the square lattice.

Although the Hubbard square is particularly illuminating as it is analytically solvable, it is worth noting that other small clusters—solvable numerically—can exhibit similar behaviors, and in particular regime pair binding arises even when U > 0. Examples of this include the Hubbard model on the tetrahedron (in which pair binding persists for all U), cube, and truncated tetrahedron (26).

Distinct phases of matter—and in particular spontaneously broken symmetries—do not arise in finite Hubbard clusters. However, in certain circumstances, the properties of an extended system

consisting of weakly coupled clusters can be inferred from the properties of an isolated cluster in a controlled expansion in powers of the (assumed small) intercluster couplings. Such an analysis was carried through for a 2D "checkerboard" array of Hubbard squares in References 27–33. Here, the complexity of the various regimes found for the isolated square implies the existence of a still richer phase diagram in the U-x plane. Not surprisingly, in the range of U for which there is pair binding on the single square, there arises a substantial portion of this phase diagram in which the ground state is a d-wave superconductor (SC)—although as a consequence of the reconstructed band structure implied by the four-site unit cell, the line of nodes fails to intersect the Fermi surface, and hence the quasiparticle spectrum is fully gapped. In addition, there is a variety of possibly insulating CDW and SDW states and several distinct Fermi liquid phases, among which is one with spin- $\frac{3}{2}$ , charge e quasiparticles (which is thus not adiabatically connected to any free electrons state) and one with quasiparticles with spin- $\frac{1}{2}$ , charge e, and an additional orbital pseudospin  $\frac{1}{2}$ .

#### 4. ONE DIMENSION

In a tour de force of mathematical physics, the 1D Hubbard chain was exactly solved by the Bethe ansatz method<sup>2</sup> (34). For this as well as for more general 1D problems, such as the Hubbard model on various relatively narrow-width ladders and cylinders, much more is known than for higher-dimensional cases. Particularly powerful numerical methods can be deployed, as discussed in Section 6.1 below. In addition, a weak coupling renormalization group (RG)—known colloquially as g-ology in reference to the various couplings  $g_a$ —leads to a rich set of results involving multiple intertwined orders in the sense that the interactions that promote CDW, SDW, and singlet and triplet superconducting correlations evolve in a complex, interrelated fashion under RG.

Furthermore, at long distances and low energies, the properties of all such 1D systems are describable by a limited set of free boson conformal field theories; i.e., the physics is that of a small number of weakly interacting, linearly dispersing bosonic collective modes. Distinct quantum phases of matter are generically classified by possible discrete broken symmetries, and by the number of gapless modes (i.e., the central charge) and the quantum numbers (spin, charge, crystalmomentum, etc.) associated with each such mode (35, 36). The relation between the microscopic fermionic degrees of freedom and the bosonic modes, called bosonization, can be complicated in specific cases, but is in principle understood in general.

Other than some of the numerical results, this intellectual block is relatively old and well known—much of it dating from the 1970s—and so is not reviewed here. For a modern treatment, see the monograph by Giamarchi (37).

#### 5. ASYMPTOTICALLY EXACT RESULTS IN SPECIAL LIMITS

#### 5.1. Weak Coupling Limit

In this section, we consider the instabilities of the Hubbard model in d > 1 in the weak coupling limit  $U/t \ll 1$ . The goal is to express the properties of the system starting from the band structure that results from diagonalizing the Hamiltonian with U = 0. Corrections to all quantities can be expressed as an asymptotic series in U/t.

**5.1.1.** Background. Clearly, at zero temperature, the radius of convergence of this series is zero, because the behavior is qualitatively distinct for  $U/t \rightarrow 0^-$  and  $U/t \rightarrow 0^+$ : When

<sup>&</sup>lt;sup>2</sup>The Bethe ansatz solution allows one to calculate the spectrum and the many-body eigenstates of the 1D Hubbard model. Calculating correlation functions is more difficult.

 $U/t \to 0^-$ , Bardeen–Cooper–Schrieffer (BCS) mean-field theory is asymptotically exact, and there is a superconducting instability below a characteristic scale  $T_{c,-} \sim \exp{[-1/(\rho|U|)]}$ , where  $\rho$  is the density of states at the Fermi energy. The superconductivity is described by an order parameter  $\Delta$ , which has only one sign on the entire Fermi surface, so that  $\langle \Delta \rangle_{FS} \simeq \max(\Delta)_{FS}$ , where  $\langle \bullet \rangle_{FS}$  denotes an average over the Fermi surface. Such a superconducting state is termed conventional as it arises in many elemental metals in which the pairing mechanism is the electron–phonon coupling. When  $U/t \to 0^+$ , as we now argue, there is also a superconducting instability, but with two qualitatively different features. First, the superconductivity itself sets in below a parametrically lower scale  $T_{c,+} \sim \exp{[-1/(\alpha \rho^2 U^2)]} \ll T_{c,-}$ , where  $\alpha$  is an order unity constant that depends on the entire band structure of the system. Second, the superconducting behavior is unconventional in the sense that  $\langle \Delta \rangle_{FS} \ll \max(\Delta)_{FS}$ .

These distinctions imply that the ground states on either side of U/t = 0 are not adiabatically connected. The point U/t = 0 is a peculiar multicritical point corresponding to a free Fermi gas. These sharply distinct asymptotic behaviors are also more directly manifest in perturbation theory at finite frequency: A subclass of perturbative corrections represented diagrammatically by ladders in the particle–particle (BCS) channel are logarithmically divergent so long as either time-reversal symmetry or inversion symmetry are present in the normal state.

In a seminal paper, Kohn & Luttinger (KL; 38) explored how superconductivity arises from repulsive interactions. They considered a three-dimensional electron gas with weak short-ranged repulsive interactions, for which they identified an instability to an unconventional superconducting state with nonzero Cooper pair angular momentum. In particular, they emphasized the role played by Friedel oscillations associated with the existence of a sharp Fermi surface. Below, we provide a modern discussion of the problem in the language of the RG, and show that (in contradistinction to the KL analysis) the structure of the particle–hole susceptibility at all energy scales, not just close to the Fermi level, determines the superconducting instabilities (39, 40). For recent reviews on superconductivity from repulsive interactions, consult References 5 and 41 and references therein.

**5.1.2. The Fermi liquid fixed point.** We first summarize the basic results of the RG formulation of Landau Fermi liquid theory, pioneered by Polchinski (42) and by Shankar (43), which are invoked in the discussion that follows. To keep things simple, we present the key results for a rotationally invariant Fermi surface. The generalization appropriate for anisotropic Fermi surfaces, relevant to crystalline systems, is discussed below.

Instead of attempting to derive a Fermi liquid from microscopics, the strategy is to proclaim a fixed point of the RG and then to analyze its stability. The fixed-point theory is similar to the action  $S_0$  in imaginary time of a free Fermi gas in d-dimensions with chemical potential  $\mu$  and energy dispersion E(k):

$$S_0 = \sum_{\alpha = \uparrow, \downarrow} \int \frac{d^d k \, d\omega}{(2\pi)^{d+1}} \, \bar{\psi}_{\mathbf{k}, \omega, \alpha} \left[ i\omega - E(\mathbf{k}) + \mu \right] \psi_{\mathbf{k}, \omega, \alpha}. \tag{9}$$

We retain frequency modes  $|\omega|$  less than a UV cutoff  $\Lambda \ll E_{\rm F}$  (having "integrated out" higher energy modes) and, thus, can linearize the dispersion as  $E(\mathbf{k}) = \mu + v_{\rm F} k_{\perp} + \cdots$ . We express the measure as  $d^d k = k_{\rm F}^{d-1} dk_{\perp} d\Omega_{\mathbf{k}}$ , where  $d\Omega_{\mathbf{k}}$  is a solid angle element on the Fermi surface,  $k_{\perp}$  is the direction of momentum perpendicular to the Fermi surface, and  $v_{\rm F}$  is the magnitude of Fermi velocity. Redefining fermion fields as  $\psi_{k,\omega} \to k_{\rm F}^{(d-1)/2} \psi_{k,\omega}$ , we arrive at the fixed-point action for a

Fermi liquid:

$$S_{\rm FL} = \sum_{\alpha=\uparrow,\downarrow} \int_{-\Lambda}^{\Lambda} \frac{d\omega}{2\pi} \, \frac{dk_{\perp} d\Omega_{k}}{(2\pi)^{d}} \, \bar{\psi}_{k,\omega,\alpha} \left(i\omega - v_{\rm F} k_{\perp}\right) \psi_{k,\omega,\alpha}. \tag{10}$$

The stability of the Fermi liquid fixed point is determined by power counting, from which one learns the following: (a) a constant shift to the kinetic energy is relevant but harmless, as it amounts to a shift in the chemical potential, and (b) all higher derivative corrections to the kinetic energy are irrelevant, and hence the kinetic energy is governed by a single parameter, the Fermi velocity  $v_{\rm F}$ .

Next, we similarly analyze the role of interactions. A key observation is that generic four-fermion interactions (and all higher-order interactions) are irrelevant at the Fermi liquid fixed point, due to the phase space restrictions imposed by the Pauli principle and the Fermi surface. This result explains in large part the ubiquity of Fermi liquids in nature (the prime example being liquid helium-3) despite the presence of strong interactions in real systems. Only under two special kinematic circumstances are interactions important. First, forward scattering interactions are exactly marginal and are incorporated into the Landau parameters. Second, the dimensionless BCS interaction  $V_{\ell}$ , where  $\ell$  labels the irreducible representation (irrep) to which the pairing channel belongs, is marginal only at tree level: One-loop corrections are logarithmically divergent. (This is directly related to the properties of the particle–particle ladders that lead to the Cooper instability for negative U discussed above.) Attractive (repulsive) interactions are marginally relevant (irrelevant). This is captured by the BCS  $\beta$  function, obtained by promoting  $\Lambda$  to a running scale  $\Lambda = \Lambda_0 \exp(-t)$ , and obtaining the flow of the coupling:

$$\beta = \frac{dV_{\ell}}{dt} = -V_{\ell}^2. \tag{11}$$

Thus, repulsive BCS interactions ( $V_{\ell} > 0$ ) weaken and attractive interactions grow, eventually leading to the BCS instability.

At this point, it may seem that the KL instability is absent, as we have just concluded that the metal is stable for repulsive interactions. However, a system with short-ranged repulsive interactions can have effective attractive interactions in some pairing channel  $\ell$ , in which case the  $\beta$  function in that channel would indicate a superconducting instability. In the case of the Hubbard model, the bare repulsive U enters only the s-wave BCS channel and is orthogonal to unconventional pairing channels (d-wave, p-wave, etc.). But as we integrate out high-energy modes, we induce attractive interactions in unconventional pairing channels (44), and the dominant one among these leads to a superconducting state.

The proper description of such effects involves a two-step RG analysis (45). In the first step, we integrate out modes in a weakly interacting metal to obtain a description along the lines of the fixed-point theory above. Then, what were formally repulsive interactions at short distances may manifest themselves as attractive interactions in certain pairing channels. In the second step, the RG flow of such couplings determines the superconducting instabilities.

**5.1.3.** Two-step renormalization group for the Hubbard model. Lattice electrons governed by the Hubbard model are far from any RG fixed point, and thus any perturbative RG in this

<sup>&</sup>lt;sup>3</sup>In a rotationally invariant system,  $\ell$  corresponds to the angular momentum channel. More generally,  $\ell$  labels the irrep of a crystallographic point group.

regime is meaningless. To overcome this apparent obstacle, we integrate out the high-energy degrees of freedom perturbatively, which is well controlled in the weak coupling limit. This is the first step of the analysis. Upon doing so, we obtain a low-energy effective theory consisting of modes within an energy cutoff  $\Lambda_0 \ll E_{\rm F}$ . Generically, the effective field theory is of the Fermi liquid form described earlier, appropriately generalized to account for crystalline anisotropy. All salient microscopic details (lattice symmetry, filling, etc.) are encoded in the shape of the Fermi surface, the magnitude of the Fermi velocity as a function of position on the Fermi surface, and the marginal perturbations of the Fermi liquid, namely the Landau parameters and BCS couplings. The choice of the cutoff  $\Lambda_0$  is largely arbitrary. It should be sufficiently small that the quasiparticle dispersion can be linearized, but it cannot be exponentially small in the couplings, where perturbation theory breaks down, as we noted above. Importantly, the final results should not depend on the choice of  $\Lambda_0$ .

At the end of the first step, we thus obtain an effective Hamiltonian of Fermi liquid form  $H_{\text{eff}} = H_0 + H_{\text{BCS}}$ , where  $H_0$  is the kinetic energy keeping just the linearized dispersion about the Fermi energy and

$$H_{\text{BCS}} = -\frac{1}{2} \sum_{\mathbf{k},\mathbf{k}'} \Gamma_{\alpha,\beta;\gamma,\delta}(\mathbf{k},\mathbf{k}') \,\psi^{\dagger}_{\mathbf{k},\alpha} \,\psi^{\dagger}_{-\mathbf{k},\beta} \,\psi_{-\mathbf{k}',\gamma} \,\psi_{\mathbf{k}',\delta}.$$
 12.

When the system of interest has spatial inversion symmetry (parity), the BCS kernel above decouples into even and odd parity channels. Constraints from the Pauli principle require that without spin-orbit coupling even (odd) parity solutions have spin of zero (one):

$$\Gamma_{\alpha,\beta;\gamma,\delta}(\mathbf{k},\mathbf{k}') = \Gamma_{s}(\mathbf{k},\mathbf{k}') \left( \delta_{\alpha\gamma} \, \delta_{\beta\delta} - \delta_{\alpha\gamma} \, \delta_{\beta\delta} \right) + \Gamma_{t}(\mathbf{k},\mathbf{k}') \left( \delta_{\alpha\gamma} \, \delta_{\beta\delta} + \delta_{\alpha\delta} \, \delta_{\beta\gamma} \right), \tag{13}$$

where the subscripts s and t denote singlet and triplet, respectively. At weak coupling, these quantities can be expressed as an asymptotic series in U/t:

$$\Gamma_{s}(\mathbf{k}, \mathbf{k}') = \frac{1}{2}U + \frac{1}{4}U^{2}\left[\chi(\mathbf{k} + \mathbf{k}') + \chi(\mathbf{k} - \mathbf{k}')\right] + \mathcal{O}(U^{3}/t^{2}),$$

$$\Gamma_{t}(\mathbf{k}, \mathbf{k}') = \frac{1}{4}U^{2}\left[\chi(\mathbf{k} + \mathbf{k}') - \chi(\mathbf{k} - \mathbf{k}')\right] + \mathcal{O}(U^{3}/t^{2}).$$
14.

The quantity  $\chi(\mathbf{k})$  is the noninteracting static particle–hole susceptibility, where from dimensional analysis it follows that  $\chi \sim 1/t$ . It is important to observe that the strength of the interaction involves both large and small momentum transfers on the Fermi surface and the full structure of the susceptibilities  $\chi$  determine the effective interaction, not just the subtle nonanalyticities of  $\chi$  associated with the sharpness of the Fermi surface.

5.1.3.1. Renormalization group flow. Having obtained the low-energy effective Hamiltonian, we now analyze the RG flow of the BCS couplings. We define a dimensionless Hermitian matrix  $g(\mathbf{k}_F, \mathbf{k}_F')$ , which is the effective interaction  $\Gamma(\mathbf{k}_F, \mathbf{k}_F')$  defined above, evaluated on the Fermi surface and weighted by the density of states in the neighborhood of the Fermi points  $\mathbf{k}_F, \mathbf{k}_F'$ :

$$g(\mathbf{k}_{\mathrm{F}}, \mathbf{k}_{\mathrm{F}}') = \frac{A_{\mathrm{F}}}{(2\pi)^d} \frac{\Gamma(\mathbf{k}_{\mathrm{F}}, \mathbf{k}_{\mathrm{F}}')}{\sqrt{v_{\mathrm{F}}(\mathbf{k}_{\mathrm{F}}) v_{\mathrm{F}}(\mathbf{k}_{\mathrm{F}}')}},$$
15.

where  $A_{\rm F} = \int d\mathbf{k}_{\rm F}$  is the (d-1)-dimensional area of the Fermi surface. The RG flows are computed by promoting the cutoff  $\Lambda_0$  to a running scale  $\Lambda \to \Lambda_0 \exp(-t)$ , and the RG equation obeyed by g is the convolution,

$$\frac{dg(\mathbf{k}_{\mathrm{F}}, \mathbf{k}_{\mathrm{F}}', t)}{dt} = -\int \frac{d\mathbf{p}_{\mathrm{F}}}{A_{\mathrm{F}}} g(\mathbf{k}_{\mathrm{F}}, \mathbf{p}_{\mathrm{F}}, t) g(\mathbf{p}_{\mathrm{F}}, \mathbf{k}_{\mathrm{F}}', t).$$
 16.

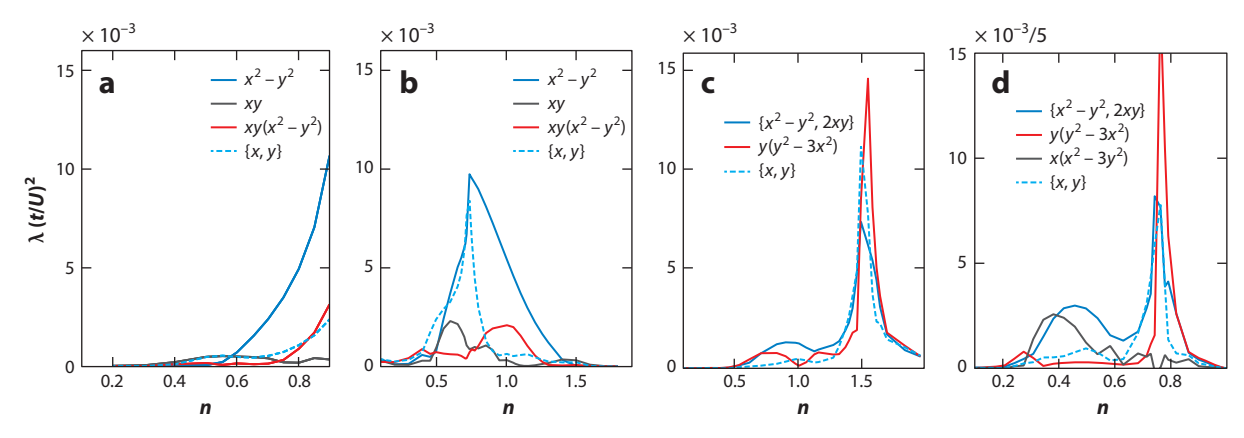


Figure 1

Dominant pairing eigenvalues  $\lambda$  (defined in Equation 17) as a function of n the density per site in the weak coupling limit of the Hubbard model on (a,b) a square lattice with second-neighbor hopping t'=0 (a) and t'=-0.3t (b), and (c) a triangular lattice, and (d) a honeycomb lattice, both with only nearest-neighbor hopping. The eigenvalues have been scaled by a factor of 5 in panel d for clarity. The dominant pairing on a square lattice near half-filling has  $d_{x^2-y^2}$  symmetry (labeled  $x^2-y^2$ ) for both t'=0 and t'=-0.3t. On the triangular and honeycomb lattices, a 2D irreducible representation with d-wave symmetry, labeled  $\{x^2-y^2, 2xy\}$ , is favored when the Fermi surface is electron-like and simply connected. By contrast, a solution with f-wave symmetry, labeled  $y(y^2-3x^2)$ , sets in near the van Hove filling and in the regime in which there are two hole-like Fermi pockets centered at the zone corners. The f-wave symmetry corresponds to a nodeless gap function with relative phase of  $\pi$  between the two hole pockets. Solutions with p-wave symmetry, labeled  $\{x,y\}$ , also occur in panels b-d in a narrow sliver of energy about the van Hove filling. This occurs when  $n \approx 0.73$  in panel b, n = 1.5 in panel c, and n = 0.75 in panel d. The figures were obtained by discretizing the Fermi surfaces at each density with a grid of 120 points. Care must be taken in the vicinity of the van Hove fillings.

It is most convenient to analyze the RG flows in the representation in which g is diagonal. Distinct eigenstates correspond to, but are not fully specified by, an irrep of the crystalline point group, where

$$\int \frac{d\mathbf{k}_{\mathrm{F}}'}{A_{\mathrm{F}}} g(\mathbf{k}_{\mathrm{F}}, \mathbf{k}_{\mathrm{F}}') \, \psi_{\ell}(\mathbf{k}_{\mathrm{F}}') = \lambda_{\ell} \, \psi_{\ell}(\mathbf{k}_{\mathrm{F}}). \tag{17}$$

Here,  $\psi_{\ell}(\mathbf{k}_{\mathrm{F}})$  is normalized such that  $\int d\mathbf{k}_{\mathrm{F}} |\psi_{\ell}(\mathbf{k}_{\mathrm{F}})|^2 = A_{\mathrm{F}}$ . Distinct eigenvalues do not mix under RG (within the one-loop approximation), and the BCS  $\beta$  function for each  $\lambda_{\ell}$  is identical in form to Equation 11.

Thus, positive eigenvalues (corresponding to repulsive effective interactions) weaken and negative ones grow. The first eigenvalue to grow to be of order unity indicates an instability of the Fermi liquid toward the corresponding superconducting state. That the bare Hubbard repulsion can generate effective attractive interactions in unconventional pairing channels is the key result of the two-stage RG analysis.

In practice, one discretizes the points on the Fermi surface and solves the resulting discrete eigenvalue problem to find the dominant eigenvalues. This way, the most important features of the band structures determine the marginal BCS couplings and the dominant instabilities. **Figure 1** shows the result for the square lattice Hubbard model with second-neighbor hopping t' = 0 (**Figure 1a**) and t' = -0.3t (**Figure 1b**). One sees that the dominant instability of the system in the weak coupling limit is to a *d*-wave SC near half-filling. In a similar fashion, one can study lattice systems of other geometries (45–47). Among other things, Reference 47 describes a plotting error in Reference 45. **Figure 1***c*,*d* shows results for the triangular and honeycomb lattices, respectively, with only nearest-neighbor hoppings. Again, near half-filling, the dominant

instability is to d-wave pairing, but in this case this corresponds to a 2D irrep, i.e., a combination of  $d_{x^2-y^2}$  and  $d_{xy}$  pairing. Determining which combination of these two components is preferred in the ordered state is beyond the scope of the RG treatment, but because the effective couplings are weak, this can be addressed within the context of BCS mean-field theory. As a consequence, one expects the corresponding superconducting state to be the time-reversal symmetry breaking combination generally referred to as  $d \pm id$ , although a nematic d-wave SC (i.e., a real combination of  $d_{x^2-y^2}$  and  $d_{xy}$ ) is also possible.

5.1.3.2. Cutoff-independence. A crucial observation described in Reference 45 was that the resulting scale associated with superconductivity is independent of the arbitrary choice of cutoff,  $\Lambda_0$ . Indeed, the only characteristic scale, namely the bandwidth W, determines the superconducting instability:  $T_c \sim W \exp(-1/\alpha \rho^2 U^2)$ , as alluded to earlier. Although the details of the proof of cutoff independence can be found in Reference 45, we provide here some intuition for why this has to be the case. The main requirement for cutoff independence is that the Fermi liquid fixed point be the only nearby fixed point. This is certainly true in the weak coupling limit.

Let us consider two different mode elimination schemes: (a) eliminating modes above the scale  $\Lambda_0$ , and (b) eliminating all modes above  $\Lambda_1 < \Lambda_0$ . The only assumptions on the cutoffs are that  $W \exp(-1/\rho U) \ll \Lambda_1 < \Lambda_2 \ll U^2/t$ . In the scheme with initial cutoff  $\Lambda_1$ , we have "less RG time" t for attractive BCS couplings to grow than the scheme with initial cutoff  $\Lambda_0$ . But this discrepancy is precisely compensated by the fact that the effective attractions start off being larger in the scheme with  $\Lambda_1$ , which is obtained by integrating the  $\beta$ -function in Equation 11 between  $\Lambda_0$  and  $\Lambda_1$ .

The presence of other nearby fixed points, or of additional modes (phonons, magnons, etc.), introduces additional scales and the cutoff independence is then no longer guaranteed. There is a corollary to this absence of any characteristic scales other than the bandwidth in the weak coupling limit: Associating a pairing glue of a well-developed bosonic fluctuation spectrum, while tempting, is strictly incorrect. Instead, the electronic fluctuation spectrum itself, at all momentum scales ranging from the lattice scale down to the longest length scales, is responsible for pairing.

**5.1.4. Extensions.** In the weak coupling limit of the Hubbard model in d > 1, the Fermi liquid state is generically unstable only to superconductivity. It is typically necessary to treat the model at intermediate or strong coupling to access nonsuperconducting orders, for instance, using the large-N or numerical approaches discussed below. To access such orders within the weak coupling limit, one has to consider nongeneric band structures, such as those that produce a perfectly nested Fermi surface or a case in which the Fermi surface crosses a 2D van Hove singularity (vHS). Although these are fine-tuned cases, they bring the interplay between superconductivity and the tendency toward other broken symmetry phases into the weak coupling regime (48).

Considerable effort has been devoted to such problems. For instance, in the case of Fermi surfaces crossing a 2D vHS, the problem has been studied in straight perturbation theory, first by Dzyaloshinskii (49) and Schulz (50), who concluded that the most singular tendency was toward superconductivity. A more sophisticated scaling theory near 2D vHS has remained elusive, as one must contend with the existence of log-squared divergences in the Cooper channel along with log divergences of forward scattering interactions. The interplay between these effects leads to RG equations that explicitly depend on the energy scale and, hence, are useless when it comes to constructing asymptotic behavior of correlation functions (for a review, see 48).

As already mentioned, the weak coupling RG in 1D is quite different than for d > 1. However, in special cases, such as for the case of quadratic band-touching in two dimensions, the RG

equations have similar form as in one dimension<sup>4</sup> (53, 54). As in the usual Fermi liquid, in these cases there are a number of interactions—represented by a set of running coupling constants,  $g_a(t)$ , that are marginal (dimensionless) by power counting. To lowest nontrivial order, this leads to a perturbative expression for the RG flows (analogous to that in Equation 16) of the form

$$\frac{dg_a}{dt} = \Gamma_a^{b,c} g_b g_c + \dots,$$
 18.

where summation convention is assumed, and the remaining terms are of third order and higher. The important point is that the tensor quantity  $\Gamma$ , which reflects physics of the specific system being studied, generally intertwines the various different interactions in a nontrivial fashion.

Depending on the specific problem being studied, and the bare values of the interactions, there are two different sorts of behavior solutions that this equation can exhibit. Under some circumstances, the interactions are all marginal or marginally irrelevant; i.e., some combinations of g's flow to zero and others do not change under RG (at least to this order). More usually, there are some sets of interactions that are marginally relevant. In this case, the RG flows carry the system to a ray along which the interactions continue to grow until, no matter how weak the bare interactions, a point is reached at which the perturbative treatment breaks down. At this point, other methods must be employed to solve the problem. The possible rays can be identified (55) by looking for possible solutions of the form  $g_a(t) = G_a(t^* - t)^{-1}$ , where  $G_a$  are solutions of the set of quadratic equations

$$G_a = -\Gamma_a^{b,c} G_b G_c. 19.$$

Those couplings for which  $G_a \neq 0$  grow strongly toward strong coupling under the RG flow, whereas any coupling for which  $G_a = 0$  remains relatively weak. Such a runaway flow of some of the coupling constants typically signals the opening of an interaction-driven gap, often associated with spontaneous symmetry breaking.

Despite the fact that these results apply (in d > 1) only for fine-tuned band structures, they may be useful over some range of intermediate energies and/or temperatures if the fine-tuned conditions are approximately satisfied, especially if one extrapolates the results to intermediate coupling strengths. We refer the reader to the literature for further discussion of these ideas (54, 56, 57).

#### 5.2. Strong Coupling Limit

When the density of electrons per site is n = 1, the low-energy physics in the strong coupling limit of the Hubbard model is, famously, that of the corresponding spin- $\frac{1}{2}$  Heisenberg antiferromagnet, with exchange coupling  $4 |t_{ij}|^2 / U$ . This applies whether the lattice is regular or irregular. At the same time, the system is a Mott insulator in the simple sense that the insulating gap,

$$\Delta_{\rm c} = \frac{1}{2}U + \mathcal{O}(t),\tag{20}$$

is determined by the interaction strength and has no relation to any ordering phenomena that occur below temperature scales of order J.

Needless to say, the physics of quantum antiferromagnets is a rich topic in its own right. Depending on the lattice structure, the range of the exchange interactions, and the degree of disorder, strong evidence points to the existence of various forms of AF ordered phases (colinear, coplanar, noncoplanar, commensurate or incommensurate, chiral or nonchiral, etc.), spin-Peierls phases, nematic and spin nematic phases, quantum spin liquid (QSL) phases of various flavors, spin-glasses, random singlet phases, and surely others.

<sup>&</sup>lt;sup>4</sup>This also applies for quadratic band-touching in three dimensions with appropriate long-range forces (51, 52).

For n < 1, the low-energy physics (e.g., the equilibrium properties of the system at temperatures  $T \ll U/2$ ) is governed by a version of the famous t–J model,

$$H_{t-J} = -\sum_{i,j} t_{ij} \hat{B}_{ij} + \sum_{i,j} J_{ij} \left( S_i \cdot S_j - \frac{1}{4} \, \hat{n}_i \, \hat{n}_j \right) - \sum_{i,j,k} K_{ijk} \, \hat{\Delta}_{ij}^{\dagger} \, \hat{\Delta}_{jk} + \mathcal{O}(t^3/U^2),$$
 21.

where  $\hat{B}_{ij} = c^{\dagger}_{i\uparrow}c_{j\uparrow} + c^{\dagger}_{i\downarrow}c_{j\downarrow}$ ,  $\hat{\Delta}_{ij} = 2^{-1/2}(c_{i\uparrow}c_{j\downarrow} + c_{j\uparrow}c_{i\downarrow})$ , and  $K_{ijk} = 2t_{ij}t_{jk}/U$ , and where it is understood that  $H_{t-J}$  operates in a restricted Hilbert space in which no site is doubly occupied. This model is often studied in its own right (typically neglecting the term proportional to K) and, so long as  $J_{ij} < |t_{ij}|$ , the results are often taken as representative of results for the Hubbard model in some physically reasonable range of  $U_{\rm eff} \sim 4t^2/J$ . However, strictly speaking, the mapping to the  $t\!-\!J$  model is valid only in the asymptotic limit  $J_{ij}/t_{ij} \to 0$ .

Thus, truly in the strong coupling limit, one should begin with the solution of the  $U \to \infty$  problem, i.e., the t-J model with  $J_{ij} = K_{ijk} = 0$ , and only keep corrections due to nonzero J and K as small perturbations. The Hubbard model was originally introduced to study itinerant ferromagnetism, based on the fact that this occurs in Hartree–Fock (HF) approximation so long as the Stoner criterion is satisfied,  $U\rho(E_{\rm F}) > 1$ . However, more accurate numerical studies have found that ferromagnetism in the Hubbard model on a bipartite lattice with  $|{\bf A}| = |{\bf B}|$  seems to require  $U\rho(E_{\rm F}) \gg 1$ . To elicit ferromagnetism for  $U/t = \mathcal{O}(1)$ , it appears necessary to introduce frustration in the form of further-neighbor same-sublattice hoppings, or to consider the model on nonbipartite lattices (58) or on line graphs (59, 60) at densities away from half-filling.

Provided the kinetic energy satisfies the Perron–Frobenius condition  $(t_{ij} \ge 0 \text{ for all } i \text{ and } j)$ , the problem with a single hole in a finite-size lattice is governed by Nagaoka's theorem (see Section 2); i.e., the ground state is a fully polarized ferromagnetic state. Clearly, the limit  $U \to \infty$  and  $N \to \infty$  do not commute. However, for large but finite U, the solution in the thermodynamic limit is a Nagaoka polaron. Its nature can be understood from a simple variational argument: Consider a state in which a region of radius R has spins aligned ferromagnetically, whereas the rest of the system is in its n = 1 AF ground state. The variational energy of such a state is

$$E_{\text{Nag}} = -E_0 + \bar{t}R^{-2} + \bar{J}R^d,$$
 22.

where  $E_0 = \sum_j t_{ij}$ , and  $\bar{t}$  and  $\bar{J}$  are averages of  $t_{ij}$  and  $J_{ij}$  that depend on the details of the lattice structure and the assumed shape of the polaron; here, the second term is the kinetic energy cost of confining the hole in a region of size R and the third term is the cost in exchange energy of making a ferromagnetic bubble. Minimizing this expression with respect to R, we obtain the following expression for the size and energy of the Nagaoka polaron:

$$E_{\text{Nag}} = -E_0 + 2\bar{t}R^{-2} \text{ with } R_{\text{Nag}} = (2\bar{t}/d\bar{J})^{1/(d+2)}.$$
 23.

It is a straightforward exercise to go from the single polaron to the problem with a small but finite hole density. The polaron should strictly be viewed as a new sort of quasiparticle—one with charge e and spin  $S \sim R_{\rm Nag}^d$ . Two such particles have a short-range effective attraction of order  $\bar{t}R_{\rm Nag}^{-2}$ ; if two are placed adjacent to each other, the hole associated with each polaron can now delocalize over twice as large a ferromagnetic region. Thus, there is a tendency for polarons to agglomerate, i.e., for the system to phase separate. Opposing this is the effective Fermi pressure of the polaron gas—however, because the polaron is large, its effective mass is large, 5 so the Fermi pressure is negligible. Thus, at T=0 and for low density of doped holes,  $1>n>n_c$ , one expects

<sup>&</sup>lt;sup>5</sup>Relative to the band mass, the Nagaoka polaron can readily be seen to have an effective mass enhancement of order  $(\bar{t}/\bar{J})R_{\mathrm{Nag}}^{d-1}$ . This is true because moving the polaron involves flipping spins along its entire surface.

macroscopic two-phase coexistence between an undoped AF phase with n=1 and a fully polarized ferromagnetic phase with  $n=n_c$ , where  $n_c \sim R_{\rm Nag}^{-d}$ . Correspondingly, for a range of densities  $n>n_c$  but not too small, this line of reasoning leads one to expect a half-metallic ferromagnetic phase, i.e., a state with all the spins parallel to one another.

The stability of the fully spin-polarized state (known as a half-metallic ferromagnet or HMF) at finite doped hole density has not been rigorously established. Indeed, it has been shown that even for  $U=\infty$ , the fully polarized state is unstable beyond a (typically substantial) critical doped hole density (61). However, exact diagonalization (62) and density-matrix-renormalization group (DMRG) studies (63) of the model on a square lattice (2D) provide strong corroborating evidence that the half-metallic ferromagnetic phase is stable for  $U=\infty$  in the range of density  $1>n \gtrsim 0.8$  and that two-phase coexistence occurs at large but finite U in a range of density  $1>n > n_c \sim (t/U)^{1/2}$ . However, there is also indication that ferromagnetic phases arise only when U is extremely large,  $U/t \gtrsim 100$ . Nonetheless, the existence of ferromagnetic phases at very large U implies that, strictly speaking, the nonferromagnetic states generally seen (and expected) at intermediate values of U cannot be approached from a strong coupling perspective.

#### 5.3. Dilute Limit

The dilute limit of the Hubbard model is defined by fixing U/t and letting  $n \to 0$ . In this limit, strong arguments have been put forward that in d = 2 and 3 and for positive U, the system forms a Fermi liquid (which may have a superconducting instability at very low temperatures, to be discussed below).

Consider d=3 first. Using the filled Fermi sea as a trial state, the kinetic energy per particle scales as  $\mathcal{E}_{\mathrm{KE}} \sim t \ n^{2/3}$  (where we have used the effective mass approximation near the band bottom), whereas the typical interaction energy satisfies  $\mathcal{E}_{\mathrm{PE}} \sim U n$ . Thus, in the limit  $n \to 0$ ,  $\mathcal{E}_{\mathrm{KE}} \gg \mathcal{E}_{\mathrm{PE}}$ . One may therefore expect the system's properties to be calculable in an expansion in the small parameter  $(U/t) \cdot n^{1/3}$  (which plays a similar role to that of  $r_s$  in a uniform electron gas). As explained in References 64–66, the proper small parameter is actually  $k_{\mathrm{F}} a_{\mathrm{s}}$ , where  $k_{\mathrm{F}} \propto n^{1/3}$  and  $a_{\mathrm{s}}$  is the scattering length. For small U/t, the scattering length satisfies  $a_{\mathrm{s}} \sim a (U/t)$  (where a is a lattice constant).

In d=2, the situation is more subtle, because the above argument gives that  $\mathcal{E}_{KE}/\mathcal{E}_{PE}$  is density independent. However, a more careful treatment (outlined below) shows that in this case the two-particle scattering amplitude near the Fermi energy, which is proportional to  $1/\ln{(1/n)}$ , serves as an emergent small parameter (65). Thus, in both cases, a systematic expansion starting from the Fermi gas is possible, resulting in a Fermi liquid whose Landau parameters are parametrically small in the  $n \to 0$  limit.

To arrive at the expansion appropriate for the dilute limit, we examine the diagrammatic representation of the two-particle vertex function. The dominant terms are the ones that form the ladder series (**Figure 2a**). Summing the ladder series gives the effective two-particle interaction (also known as the T-matrix):

$$U_{\text{eff}}(q,\epsilon) = \frac{U}{1 + \Gamma_0(q,\epsilon)U},$$
 24.

 $<sup>^{6}</sup>$ It is a peculiarity of the Hubbard model that there is no interaction between electrons with the same spin—thus, for any value of n, all energy eigenstates with maximal total spin are simply Slater determinants. In particular, the half-metallic ferromagnetic ground state is always an eigenstate of the Hubbard Hamiltonian—the only question is under what circumstances it is the ground state.

Figure 2

(a) Ladder series for the two-particle scattering amplitude in the dilute limit. The empty square represents the bare interaction U, and the filled square is the effective interaction  $U_{\rm eff}$  (also known as the T matrix). (b,c) Examples of diagrams that are not part of the ladder series. These diagrams are suppressed, in the  $n \to 0$  limit, compared to those shown in panel a.

where  $\Gamma_0(q,\epsilon) = \int \frac{d^dk}{(2\pi)^d} (\varepsilon_k + \varepsilon_{-k+q} - i\epsilon)^{-1}$ . In the dilute limit, we are interested in the interaction at momenta and energies of the order of the Fermi momentum and Fermi energy, respectively. In d=3, we can safely take  $|q|\to 0$  and  $\epsilon\to 0$ , obtaining  $\Gamma_0\sim 1/t$ . Terms that are not part of the ladder series, such as those shown in **Figure 2**(b,c), are suppressed by powers of  $\rho U_{\rm eff}\sim k_{\rm F} a_{\rm s}$  and are thus small. The effective interaction near the Fermi energy is thus finite in the dilute limit. The Fermi liquid parameters, such as the Landau function and the effective mass correction, are all of the order of  $k_{\rm F} a_{\rm s}$  (because they are proportional to  $\nu_0 \propto k_{\rm F}$ ). The smallness of the Fermi liquid parameters ensures the self-consistency of the expansion.

In d=2,  $\Gamma_0$  diverges logarithmically in the limit  $|q|\to 0$ ,  $\epsilon\to 0$ . This divergence is cut off by setting  $|q|\sim k_{\rm F}$  and  $\epsilon\sim \mu$ , where  $\mu$  is the chemical potential. In the dilute limit, such that  $(U/t)\ln{(1/n)}\gg 1$ , this gives  $U_{\rm eff}\sim t/\ln{(t/\mu)}\sim t/\ln{(1/n)}$ . Hence, terms that are not part of the ladder series are suppressed by a factor  $\rho U_{\rm eff}\sim 1/\ln{(1/n)}\ll 1$  and can be neglected (65). The Fermi liquid parameters are small in proportion to  $1/\ln{(1/n)}$ .

In both d = 2 and d = 3, the system is thus described as a weakly interacting Fermi liquid in the dilute limit, independent of the original Hubbard interaction. The Fermi liquid state can then be treated as discussed in Section 5.1. In d = 3, and in the presence of time-reversal or inversion symmetries, one expects an instability toward a triplet superconducting state whose critical temperature  $T_c$  scales as

$$E_{\rm F} e^{-1/(\rho U_{\rm eff})^2} \sim t \, n^{2/3} \, \exp\left\{-\left(1 + \frac{t}{U}\right)^2 n^{-2/3}\right\},$$
 25.

where we have omitted dimensionless numbers of the order of unity in the exponents. The d=2 case requires additional care, because the Lindhard susceptibility is nearly momentum independent. Hence, no effective attraction is generated at second order in  $U_{\rm eff}$ . A calculation of the third-order terms, performed in Reference 67, gives  $T_{\rm c} \sim E_{\rm F} \exp[-1/(\rho U_{\rm eff})^3] \sim t \, n \exp[-1/\ln^3(1/n)]$ . Note that in both d=2 and 3,  $T_{\rm c} \ll E_{\rm F}$ .

#### 5.4. Large-N Generalization and the Hartree-Fock Approximation

Although quantum many-body models are generally insoluble except in very special cases, by extending the global symmetry of the model from SU(2) to a larger group such as SU(N) or Sp(N), a systematic expansion in powers of 1/N about the  $N \to \infty$  limit can often be derived (68–73). Here, we discuss a large-N generalization of the Hubbard model (74) that allows controlled access

to a variety of intermediate coupling spin and charge ordered phases. Consider the Hamiltonian

$$H = -\sum_{\langle ij \rangle} \sum_{\alpha=\pm}^{N} \sum_{m=1}^{N} c_{i\alpha m}^{\dagger} (t_{ij} + \mu \, \delta_{ij}) c_{j\alpha m} + \frac{1}{N} \sum_{i} (\frac{1}{2} V n_{i}^{2} - \frac{1}{2} J S_{i}^{2} + \frac{1}{2} K \Psi_{i}^{\dagger} \Psi_{i}), \qquad 26.$$

where i labels the lattice sites,  $\alpha = \pm$  the spin polarization, and  $m \in \{1, ..., N\}$  is a flavor index. The coupling constants V, J, and K are all nonnegative. The local density  $n_i$ , spin  $S_i$ , and superconducting order parameter  $\Psi_i$  are given by

$$n_{i} = \sum_{\alpha,m} c_{i\alpha m}^{\dagger} c_{i\alpha m}, \quad S_{i} = \frac{1}{2} \sum_{\alpha,\beta,m} c_{i\alpha m}^{\dagger} \sigma_{\alpha\beta} c_{i\beta m}, \quad \Psi_{i} = \sum_{\alpha,\beta,m} c_{i\alpha m} \epsilon_{\alpha\beta} c_{i\beta m}, \quad 27.$$

where  $\epsilon_{\alpha\beta} = i\sigma_{\alpha\beta}^{\gamma}$ . Consider a global transformation of the fermion fields,

$$c_{i\sigma m} \to \widetilde{c}_{i\sigma m} = \mathcal{R}_{mm'} \mathcal{U}_{\sigma\sigma'} c_{i\sigma'm'}.$$
 28.

Suppressing the site index i, we write  $\tilde{c} = \mathcal{R} \mathcal{U} c$ , where  $\mathcal{R}$  acts on flavor indices and  $\mathcal{U}$  acts on spin indices. Thus,

$$\widetilde{n} = c_{\sigma m}^{\dagger} (\mathcal{R}^{\dagger} \mathcal{R})_{mm'}, (\mathcal{U}^{\dagger} \mathcal{U})_{\sigma \sigma'} c_{\sigma' m'},$$

$$\widetilde{S}^{u} = \frac{1}{2} c_{\sigma m}^{\dagger} (\mathcal{R}^{\dagger} \mathcal{R})_{mm'} (\mathcal{U}^{\dagger} \sigma^{u} \mathcal{U})_{\sigma \sigma'} c_{\sigma' m'},$$

$$\widetilde{\Psi} = (\mathcal{R}^{t} \mathcal{R})_{mm'} (\mathcal{U}^{t} \epsilon \mathcal{U})_{\sigma \sigma'} c_{\sigma n} c_{\sigma' n'}.$$
29.

Thus, if  $\mathcal{U} \in SU(2)$  and  $\mathcal{R} \in O(N)$ , we have  $\widetilde{n} = n$  and  $\widetilde{\Psi} = \Psi$ , and furthermore  $\widetilde{S}^a = M_{ab} S^b$ , where  $M_{ab} = \frac{1}{2} \operatorname{Tr}(\mathcal{U}^{\dagger} \sigma^{a} \mathcal{U} \sigma^{b}) \in SO(3)$ . Hence,  $\widetilde{H} = H$ ; i.e., the Hamiltonian H possesses a global  $U(2) \times O(N)$  symmetry [including the U(1) charge conservation]. In the case N = 1, the system reduces to the usual Hubbard model with  $U = V + \frac{3}{4}J + 2K$ .

To elicit the large-N theory, we employ three Hubbard-Stratonovich transformations to decouple each of the three terms quartic in the fermion operators. The resulting dimensionless action is then

$$A = \int_{0}^{\beta} d\tau \sum_{i} \left( \frac{N}{2V} \phi_{i}^{2} + \frac{N}{2J} \chi_{i}^{2} + \frac{N}{2K} |\Delta_{i}|^{2} \right) + \sum_{\substack{i,j \ \sigma,m}} \bar{c}_{i\sigma m} \left( \partial_{\tau} - t_{ij} - \mu \delta_{ij} \right) c_{j\sigma m}$$

$$- \frac{1}{2} \sum_{i,m} \sum_{\alpha,\beta} \left[ \bar{c}_{i\alpha m} c_{i\alpha m} \right] \begin{bmatrix} i\phi_{i} \delta_{\alpha\beta} + \frac{1}{2} \chi_{i} \cdot \sigma_{\alpha\beta} & i\Delta_{i} \epsilon_{\alpha\beta} \\ i\bar{\Delta}_{i} \epsilon_{\alpha\beta} & -i\phi_{i} \delta_{\alpha\beta} - \frac{1}{2} \chi_{i} \cdot \sigma_{\alpha\beta} \end{bmatrix} \begin{bmatrix} c_{i\beta m} \\ \bar{c}_{i\beta m} \end{bmatrix}.$$
30.

Here,  $\beta = 1/k_B T$ , where T is the temperature,  $\tau$  is imaginary time, and  $\{\phi_i, \chi_i, \text{Re } \Delta_i, \text{Im } \Delta_i\}$  are the six time-dependent Hubbard-Stratonovich fields.

We may now formally integrate out the fermions, obtaining the following effective action:

$$A_{\text{eff}} = \int_{0}^{\beta} d\tau \sum_{i} \left( \frac{N}{2V} \phi_{i}^{2} + \frac{N}{2J} \chi_{i}^{2} + \frac{N}{2K} |\Delta_{i}|^{2} \right) - \frac{1}{2} N \operatorname{Tr} \log \mathcal{G}^{-1}[\{\phi_{i}\}, \{\chi_{i}\}, \{\Delta_{i}\}].$$
 31.

Here,  $\mathcal{G}^{-1} = \mathcal{G}_0^{-1} - \mathcal{M}[\{\phi_i\}, \{\chi_i\}, \{\Delta_i\}],$  where

$$\mathcal{G}_0^{-1} = \begin{bmatrix} G_0^{-1} & 0\\ 0 & -\left(G_0^{-1}\right)^T \end{bmatrix}.$$
 32.

The inverse of the free Green's function is given by  $G_0^{-1} = -\partial_\tau + t_{ij} + \mu \delta_{ij}$ , and  $\mathcal M$  is the matrix that appears in the second line of Equation 30.

Crucially, the effective action is proportional to N. Hence, in the large N limit, the partition function is dominated by the lowest-action saddle point of  $A_{\rm eff}$ . Fluctuations around the saddle point are suppressed by powers of  $N^{-1}$ . We seek a saddle point characterized by time-independent, but possibly site-dependent, fields  $\phi_i$  and  $\chi_i$ . Because we have assumed  $K \geq 0$ , it is straightforward to see that  $\Delta_i = 0$  at any such saddle point. Substituting  $\widetilde{\phi}_i \equiv i\phi_i$  and differentiating the effective action with respect to  $\widetilde{\phi}_i$  and  $\chi_i$  yields

$$\begin{split} \widetilde{\phi}_i &= -V \sum_{\alpha,m} \left\langle \bar{c}_{i\alpha m} \, c_{i\alpha m} \right\rangle_{\widetilde{\phi}_i, \mathbf{X}_i}, \\ \mathbf{\chi}_i &= \frac{1}{2} J \sum_{\alpha,\beta,m} \left\langle \bar{c}_{i\alpha m} \, \sigma_{\alpha \beta} \, c_{i\beta m} \right\rangle_{\widetilde{\phi}_i, \mathbf{X}_i}. \end{split}$$
 33.

Here, the expectation value is taken with respect to the quadratic action (Equation 30) with  $\{\widetilde{\phi}_i\}$  and  $\{\chi_i\}$  set to their saddle point values. Equations 33 are the self-consistent HF equations describing possible spin and charge ordered states. They are identical to the HF equations of the one-band Hubbard model with  $2V = \frac{1}{2}J = U$  and K = 0. Thus, the HF approximation becomes asymptotically exact in the large-N generalization of the Hubbard model given by Equation 26.

**5.4.1. Some Hartree–Fock results.** There have been numerous HF studies of the Hubbard model. A priori—especially when dealing with forms of order that only arise when *U* exceeds a finite critical value—there is no obvious small parameter that justifies these solutions. However, with the large *N* limit as justification, it is worth summarizing at least some of the HF results that have been obtained in this way.

In the case of a half-filled band, n=1, with t'=0, the Fermi surface is perfectly nested and the HF ground state is a Néel AF insulator (AFI) for all U>0. In particular, for d>2 and small U, the sublattice magnetization, m, and the quasiparticle gap,  $\Delta_{\rm AF}$ , depend on U as  $m\sim\Delta_{\rm AF}\sim\exp(-1/\rho U)$ , whereas for d=2 the expressions are slightly more complicated, with  $m\sim\Delta_{\rm AF}\sim\exp(-\sqrt{8\pi^2t/U})$ , because of the logarithmically divergent density of states associated with the van Hove points. For small but nonzero t', the system remains metallic for  $U<U_{\rm c}$  but is AF for larger U, where  $U_{\rm c}\sim t/\ln|t/t'|$  for d>2 and  $U_{\rm c}\sim t/\ln^2|t/t'|$  in d=2. The details of the metal–insulator transition as a function of U has not been exhaustively studied and may vary, depending on dimensionality, the value of t' and other details. The simplest cases involve either a direct first-order transition from a featureless metal for  $U<U_{\rm c}$  to an AF insulator for  $U>U_{\rm c}$  or a sequence of two transitions, the first (typically continuous) from a featureless metal for  $U<U_{\rm c}$  to an AF metal phase—i.e., with m small enough that a portion of the Fermi surface remains ungapped—followed by a (typically first order) transition to the AF insulator at  $U>U_{\rm c}>U_{\rm c}$ 1.

It is also interesting to consider the evolution of the HF ground state with the introduction of a dilute concentration of doped holes,  $x \equiv 1-n \ll 1$ , starting from the AFI. One possible solution of the HF equations is simply a doped version of the Néel state—here the energy cost per doped hole is  $\Delta_{\rm AF}\left[1+\mathcal{O}(x^{2/d})\right]$ . This is typically never the lowest energy HF solution (76); a better solution is one in which a portion of the sample is undoped antiferromagnet and another is a nonmagnetic metal with a finite concentration  $x_{\rm c}$  of doped holes, where  $x_{\rm c} \sim \rho(E_{\rm F}) \, \Delta_{\rm AF}$ . For small U in d>2, it was shown in Reference 76 that  $x_{\rm c}=\sqrt{2}\,\rho(E_{\rm F})\,\Delta_{\rm AF}$  and that the energy per

<sup>&</sup>lt;sup>7</sup>Interestingly, setting N=1, this choice of parameters corresponds to a Hubbard model with an interaction strength  $V+\frac{3}{4}J+K=2U$ . This discrepancy between the HF equations for the Hubbard model and the saddle point equations obtained by decoupling the interaction in an SU(2) symmetric way was noted in Reference 75.

doped hole is  $2^{-1/2}\Delta_{AF}\left[1+\mathcal{O}(x_c^{2/d})\right]$ ; i.e., it has lower energy than the doped Néel state. The same analysis applies for small t' in d=2, and even for t'=0 with slight complications owing to the divergent density of states. However, more interesting insulating states were found (77–79) to have still lower energies—at least in d=2 with t'=0. Here for small x, the system forms a unidirectional SDW state in which the doped holes are localized on antiphase domain walls a distance W apart, resulting in a new periodicity of the spin order  $\lambda=2W$ . Furthermore, the domain-wall spacing is such that there are an even-integer number of electrons per unit cell, i.e.,  $\lambda=1/x$ , and the system remains insulating. From numerics in two dimensions with t'=0, the energy per doped hole of the striped phase was estimated (80) to be approximately  $0.66 \Delta_{AF}$ , which is some 7% less than that of the phase separated state.

#### 6. NUMERICAL RESULTS

#### 6.1. Density-Matrix-Renormalization Group Results for Ladders and Cylinders

The DMRG approach (81, 82) has proven to be extremely useful in obtaining ground state correlations of Hubbard cylinders and ladders. As the computational effort grows roughly linearly with the length of the system, *L*, but exponentially with the number of legs, *W*, these results are largely confined to rather small *W*. However, for these systems, it provides an incomparably versatile approach to the intermediate coupling problem without relying on any artificial limiting procedure.

**6.1.1.** The utility of density-matrix-renormalization group. DMRG is now understood to be an extremely clever variational approach (82, 83) for studying the ground state properties of arbitrary interacting electron models. It uses a class of variational states known as matrix-product states—which, as the name suggests, are parameterized by the elements of a matrix associated with each site. The larger the dimension of the matrices (known as the bond dimension), the better the approximate ground state obtained. For any finite-size system, DMRG calculations in principle converge to the exact result for large enough bond dimension,  $B_d$ . However, as the calculations are more demanding for larger  $B_d$ , not all published results can be taken at face value. This is reflected in the unfortunate fact that there are examples in the literature of DMRG studies that have reached contradictory conclusions concerning the character of the ground state phase of certain model problems. Furthermore, different sorts of results require different levels of care (84), as we elaborate below.

- Generally, the bond dimension required to achieve a given accuracy increases exponentially with the degree of entanglement of the phases being explored. Thus, DMRG results converge more easily in systems in which the central charge (the number of gapless modes) is small and all correlation lengths are short. Conversely, systems with many gapless modes and/or long correlation lengths may need a very large  $B_d$  to converge.
- Even within a given phase, the reliability of the DMRG results for fixed  $B_d$  depends, to some extent, on what questions are asked. The nature of the short-range correlations—i.e., what sort of local order arises—is less sensitive to subtle aspects of the entanglement and, so, can be extracted reliably even in calculations with relatively modest values of  $B_d$ , whereas issues concerning long-distance correlations—especially power-law falloff of correlations associated with gapless modes—are much more strongly dependent on  $B_d$ .

In quoting results of DMRG calculations, we have restricted ourselves to discussing results either that pertain to short-range correlations (about which there typically is no disagreement) or in which the  $B_d$  dependence has been seriously investigated and the extrapolation to  $B_d \to \infty$  appears

convincing. There are also generalizations of DMRG, such as projected entangled pair states (85), which uses tensorial generalizations of the matrix product states of DMRG. Because these methods have not been as thoroughly tested and benchmarked as has DMRG, we have largely omitted results obtained from these approaches. DMRG methods have recently been extended and are beginning to be applied to study dynamical properties of ladders and cylinders (86, 87). This is a very promising new direction but one that is still in its infancy. Again, taking a conservative stance, we have mostly not reviewed these results (see, however, Reference 2 in this volume).

The bulk of the DMRG studies have been carried out on ladder or cylinder versions of the Hubbard model for intermediate values of U on the order of the bandwidth,  $8t \le U \le 12t$ , and for ranges of electrons per site n in the range  $1.3 \ge n \ge 0.7$ , corresponding to a concentration of doped holes or doped electrons  $0 \le x \le 0.3$ . Effects of differing band structure have been studied largely by considering a range of first- and second-neighbor hopping, t'/t. Many studied have treated the t-J instead of the Hubbard model, because the results for the former tend to have better convergence properties. Results so obtained are generally interpreted as representative of the solutions of a corresponding Hubbard model with  $U/t \approx (4t/J)$  and a somewhat renormalized value of t'/t.

We now summarize some of the salient results that have been obtained from these studies. We distinguish the following three types of inferences that can be drawn:

- 1. Most directly, from an analysis of the short-distance behavior of various ground state correlation functions, it is relatively straightforward to determine what sort of ordering tendencies are strong for particular ranges of parameters. We illustrate such orders by describing the form of broken symmetry (long-range order) that would result were these short-distance correlations extended to long distances. Because the Hubbard model is not a realistic model of any actual material, it may be that identifying ordering tendencies reveals the most model independent—and, hence, physically significant—features of the interesting strong correlations physics.
- 2. Extrapolating the result to the limit of infinitely long cylinders and ladders, we can identify distinct phases of matter based on the asymptotic long-distance correlations. As discussed in Section 4, this means identifying any discrete broken symmetries, and the number and character of distinct gapless charge and spin modes; for instance, a Luther–Emery liquid has a single gapless charge mode (central charge c=1), and power-law quasi-long-range order CDW and superconducting correlations.
- 3. Most speculatively, we can introduce conjectures concerning the extrapolation of the DMRG results to the 2D  $(W \to \infty)$  limit. This can only be done with confidence when the results are weakly W dependent even for relatively small W.
- **6.1.2.** The square lattice. Most commonly, DMRG investigations have focused on the square lattice Hubbard and t J models. Band structure effects are sometimes modeled by the introduction of a second-neighbor hopping t'.
- 6.1.2.1. Undoped ladders. For the most part, studies of the undoped model (x = 0) have been carried out in the regime in which U is (assumed) large enough that there is a substantial charge gap,  $\Delta_c \gtrsim t$ , so the Hubbard model is equivalent to a spin 1/2 Heisenberg model with first- and second-neighbor exchange couplings,  $J/J = (t'/t)^2$ . For even W, this necessarily results in a fully gapped state (88, 89), i.e., with a nonzero spin-gap,  $\Delta_s$ .

However, for  $J'/J < X_{c1} \approx 0.41$ , the resulting state exhibits the same local spin correlations as the Néel state shown in **Figure 3***a*, and has a spin correlation length that grows exponentially with

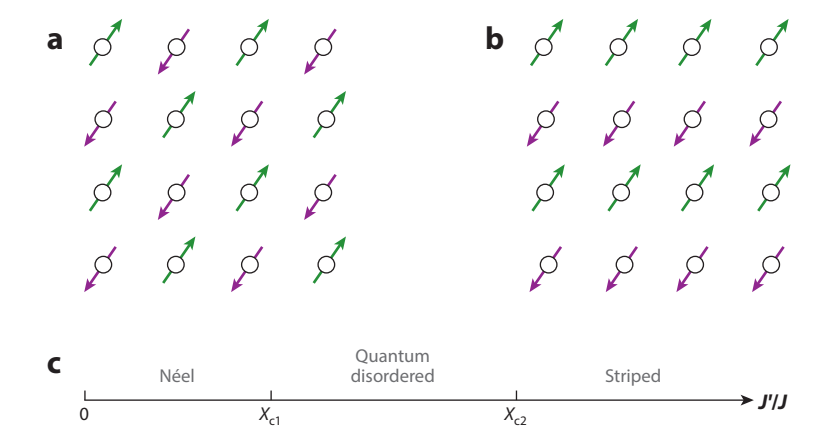


Figure 3

Forms of antiferromagnetic order in the undoped square lattice: (a) Néel, (b) stripe antiferromagnet, (c) schematic phase diagram of the 2D model at large U as a function of  $J'/J \equiv (t'/t)^2$ .

W, i.e.,  $\xi_s \sim \exp(\alpha W)$  with  $\alpha = O(1)$  (90). Indeed, as shown on theoretical grounds in Reference 89, in a range of J/J in which the 2D system has long-range AF order characterized by a renormalized spin-stiffness  $\rho_s$  and a spin-wave velocity c,  $\alpha(J/J) = 2\pi \rho_s/\hbar c$ . Thus, the DMRG results provide compelling evidence that the 2D system has Néel order in this regime, as shown in **Figure 3**c.

For  $J/J > X_{c2} \approx 0.62$ , the local order resembles the stripe magnetic state, shown in **Figure 3b**. Although we have not found data that show the systematic scaling of  $\xi_s$  with W,  $\Delta_s$  is a sufficiently rapidly decreasing function of W up to at least W = 10 that it is reasonable to conclude that stripe long-range order arises in the  $W \to \infty$  limit. By contrast, for  $X_{c1} < J'/J < X_{c2}$ , there is a spin-gap that does not decrease substantially with increasing W. These results have led to the conjecture (90, 91) that, for this intermediate range, there is a quantum disordered phase or phases (i.e., phases with no magnetic order) in the  $W \to \infty$  limit, as shown in **Figure 3c**. However, there is still some debate (92) about the nature of this region in the 2D limit, e.g., whether there is valence bond crystalline order or a  $\mathbb{Z}_2$  QSL.

**6.1.2.2.** Lightly doped ladders. DMRG studies of the doped ladder have also primarily involved U large enough that the undoped ladder is insulating and have focused on the range of parameters (i.e.,  $J/J < X_{c1}$ ) that correspond to a doped Néel antiferromagnet.

Naturally, the most reliable results have been obtained for the two-leg ladder, W=2. So long as  $x < x_{\rm c} \sim 0.3$ , for the typical range of intermediate U and t'/t, there is general consensus (93–96) that, in the  $L \to \infty$  limit, such ladders generically form a Luther–Emery liquid (97). Specifically, there is a nonzero spin-gap,  $\Delta_{\rm s} \sim t^2/U$ , and a single gapless charge mode (c=1) and power-law equaltime CDW and SC correlations that falls as  $\cos(Q_{\rm CDW}r+\phi_0)|r|^{-K_{\rm CDW}}$  and  $|r|^{-K_{\rm SC}}$ , respectively. The CDW ordering vector is equal to the value of  $2k_{\rm F}=W\pi n$  mandated by the generalized LSM theorem (see Section 2),  $Q_{\rm CDW}=W\pi n\equiv 2\pi x$ , and consistent with expectations from conformal field theory,  $K_{\rm SC}=1/K_{\rm CDW}$ .

Although DMRG does not directly yield information concerning the susceptibility, once the identification with the corresponding quantum field theory is established, it follows that these same exponents can be identified with the low T behavior of the corresponding susceptibilities, i.e.,  $\chi_{\rm CDW}(q=Q_{\rm CDW})\sim T^{-(2-K_{\rm CDW})}$  when  $K_{\rm CDW}<2$  and  $\chi_{\rm SC}(T)\sim T^{-(2-K_{\rm SC})}$  if  $K_{\rm SC}<2$ . However, though both exponents are typically in the range  $2>K_{\rm SC}>1/2$  in which both susceptibilities

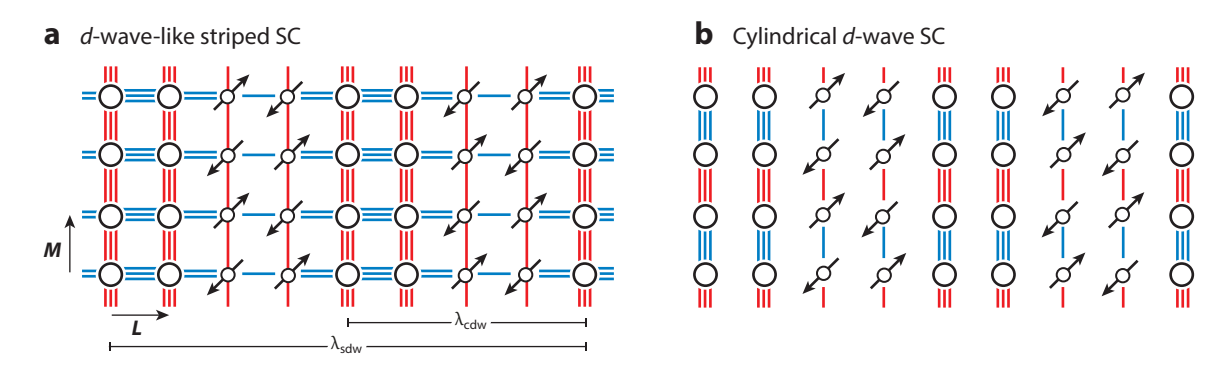


Figure 4

Various patterns of intertwined short-range order for the square lattice Hubbard model at moderate x and intermediate U. Here, the size of the circles represents the doped hole density, the arrows represent the site magnetization, and the thickness of the lines represents the magnitude of the singlet pair field on each bond; the sign of the pair field is color coded with red being positive and blue being negative. Here, panel a represents coexisting SDW, CDW, and d-wave-like SC; panel b (relevant in particular to the M=4 leg cylinder) represents SDW, CDW, and cylindrical SCs (sometimes called "true d-wave"; 106). The cylinder axis is taken to be horizontal. Abbreviations: CDW, charge-density wave; PDW, pair-density wave; SC, superconductor; SDW, spin-density wave.

diverge, the precise values of these exponents, and thus whether SC or CDW correlations are dominant, varies as a function of x and t'/t. In fact, for the two-leg ladder, the same Luther–Emery phase has been shown to exist down to U as small as U=4t. To get an idea of why smaller values of U present such difficulties, note that for t'=0 and x=1/12, the spin correlation length  $\xi_s \approx 30$  lattice constants; it is thus found that ladders up to L=200 must be treated to get reliable results (96). (Interestingly, in this case, the CDW and SC susceptibilities are equally divergent,  $K_{\rm SC} \approx K_{\rm CDW} \approx 1$ .)

The nature of the short-range correlations on the two-leg ladder are also interesting. Although the SDW correlations decay exponentially with distance, the spin correlation length is sufficiently long that one can identify a preferred ordering vector,  $Q_{\rm SDW} = \pi n \equiv \pi \pm \pi x$ . Importantly, this is mutually commensurate with the CDW ordering vector,  $Q_{\rm CDW} \equiv 2Q_{\rm SDW}$ . Also, the superconducting order is d-wave-like in the sense that the pair-field correlations on bonds parallel to and perpendicular to the ladder direction have opposite signs. (Because the ladder does not have any symmetry relating parallel and vertical bonds, this is not a precise symmetry classification, and indeed the magnitude of the pair-field correlations are somewhat different on the two sets of bonds.) The short-range order is thus a two-leg version of the correlations shown schematically in **Figure 4a**, where for graphical simplicity we have drawn this picture for the commensurate case x = 1/4 so that  $\lambda_{\rm CDW} = 4$ . The relative phase of the CDW, SDW, and SC modulations are representative of what is seen in the calculations, i.e., the spin order is strongest where the SC order is weakest and where the local doped hole concentration is closest to 0. (The fact that the CDW is bond-centered, i.e., that it preserves reflection symmetry about a bond-centered mirror plane, was likewise chosen for purposes of illustration only.)

Even for the two-leg ladder, there are circumstances in which other phases arise. As already mentioned in Section 5.2, for large enough U, for  $0 < x \lesssim 0.2$ , there is a fully polarized (half-metallic) phase; this result was also established using DMRG (63). Furthermore, for special rational values of x (such as x = 1/8) and for a range of U/t, commensurate CDW long-range order is possible (98, 99), i.e., a discrete breaking of the translational symmetry. The ordering vector in this case is, as before,  $\lambda_{\text{CDW}} = 2/x$ , but now there is a gap to charge excitations as well as a spin-gap.

Moving to W=4 leg ladders and cylinders, a still richer variety of behaviors has been observed (100–102). In particular, the nature of the states for a given value of x is found to depend significantly on the value of t'. Under some circumstances, especially in four-leg cylinders with t' small and negative, there appears to be (103–105) a Luther–Emery liquid phase with c=1, divergent CDW and SC susceptibilities with the product  $K_{\rm CDW}K_{\rm SC}=1$  and with the  $K_{\rm SC}$  in the range of  $0.5 < K_{\rm SC} \lesssim 2$ , and exponentially falling SDW correlations with  $\xi_{\rm sdw} \sim 10$ . Where this occurs, it is typically also true that  $Q_{\rm CDW}=4\pi x$ . The sketch in **Figure 4b** is a caricature of the shortrange order seen here. Recalling that periodic boundary conditions have been enforced around the cylinder, it is apparent that the SC order—which oscillates in sign between neighboring bonds around the cylinder—has a true d-wave form (105, 106) in the sense that it changes sign under a  $C_4$  rotation about the central axis of the cylinder. Such a state is likely to be a peculiarity of the four-leg cylinder.

For t'=0, the W=4 leg cylinder shows significantly different tendencies. The most extensive studies (103, 105–107) have been carried out primarily for the (assumed representative) value of x=1/8. Here, the preferred CDW ordering vector is half what it was in the previous case,  $Q_{\rm CDW}=2k_{\rm F}\equiv 2\pi x$ . Furthermore, it seems that the SC correlations fall rapidly—most probably exponentially—with distance. (However, in this case, the SC correlation length,  $\xi_{\rm SC}$  is remarkably long—it is estimated in Reference 108 that  $\xi_{\rm SC}\approx 18$ ). There is again significant short-range SC and SDW order, with, as in Figure 4a, the SC order being d-wave-like, and the SDW ordering vector satisfying the mutual commensurability condition,  $2Q_{\rm SDW}\equiv Q_{\rm CDW}$ . This, if extrapolated to the 2D limit, is suggestive (107) of a commensurate unidirectional CDW insulating state, either with or without accompanying SDW order, with a significant but strictly short-range correlated tendency toward a d-wave SC. Thinking of the peaks in the CDW as being a stripe of high doped hole density, this state, which arises naturally in HF calculations in two dimensions, is sometimes referred to as having full stripes—full in the sense that because  $\lambda_{\rm CDW}=1/x$ , there is one doped hole per site along the length of each stripe. By contrast, the state with  $\lambda_{\rm CDW}=1/2x$  (i.e.,  $Q_{\rm CDW}=4\pi x$ ) is then referred to as half-filled stripes.

Patterns of local order corresponding to partially filled stripes of different varieties have been found in calculations on W=6 leg ladders (109, 110). Very recently, there have been the first DMRG studies (111–113) (actually, of the t–J model) to find direct evidence of (quasi-)long-range d-wave-like SC order in cylinders with W>4. Not surprisingly, the SC correlations tend to be strongest for values of the parameters (e.g., t'/t) for which the CDW correlations are relatively weaker (112, 113). Generally, the phases with strong SC correlations occur only for x greater than a (parameter dependent) critical value of x—the one exception to this (111) being the case of very large  $t'\approx t/\sqrt{2}$ , where the state at x=0 is (as already discussed) a quantum para-magnet (probably a spin liquid), and where SC quasi-long-range-order appears down to the smallest values of x (x=1/18) explored so far. A periodic modulation of the hopping was found to significantly enhance the d-wave-like pairing correlations as well (114). As these are very new results, it is still necessary for further studies to be carried out to determine the full phase diagram.

**6.1.3.** The honeycomb lattice. DMRG studies have been performed for the Heisenberg model on the honeycomb lattice for a range of J/J (115, 116). The behavior of the honeycomb model has motifs similar to the more studied square and triangular lattices. In particular, there is evidence for an intermediate spin-disordered phase for a range of J/J between the Néel and striped phases. All

<sup>&</sup>lt;sup>8</sup>In DMRG studies, a value of  $t' \approx -0.3t$  is often taken as a value representative of the band structure of the hole-doped cuprates.

or much of this intermediate phase seems to possess plaquette order (116). Some DMRG studies have also been performed on the honeycomb Hubbard model away from half-filling (117–119). We do not further summarize these results here.

**6.1.4.** The triangular lattice. DMRG studies of the Hubbard model on the triangular lattice have recently produced evidence of a number of intriguing behaviors (120–125). Unfortunately, there is still considerable disagreement in the inferences drawn from different studies, making it difficult to give a definitive review.

6.1.4.1. Undoped cylinders. Undoped cylinders with  $3 \le W \le 5$  have been studied at x = 0. There is strong evidence (and a general consensus) that there are at least three distinct phases as a function of U/t. For  $U < U_{c1} \approx 8t$  there is a compressible phase that has been identified as metallic in several DMRG studies. More specifically, the DMRG studies have concluded that it is metallic in the sense of being adiabatically connected to the noninteracting limit, i.e., that there are gapless spin and charge modes corresponding to each Fermi surface crossing of the noninteracting band structure. This conclusion is difficult to reconcile with a weak coupling analysis (96) of the sort described in Section 5.1. Rather, assuming there are no as yet undetected transitions with a critical value of  $U < U_{c1}$ , it is likely that most of these modes are gapped, but that the gaps are sufficiently small (the correlation lengths sufficiently large) that they have been overlooked in DMRG studies to date. Indeed, the weak coupling analysis suggests that the small U phase is a Luther–Emery liquid (c = 1) with time reversal symmetry breaking—i.e., an extension of the d + id SC phase that arises in two dimensions at small U (see Section 5.1) to a cylindrical geometry.

The most intriguing phase at x=0 occurs for  $U_{\rm c1} < U < U_{\rm c2} \approx 10t$ . Here there is evidence that the system becomes a spin liquid in the 2D limit. For instance, for M=4 and suitable boundary conditions, there seems to be a fully gapped state with only very short-range spin correlations. It was concluded in Reference 121 that this phase is chiral—indicating that in the 2D limit it would correspond to a time reversal symmetry breaking chiral spin liquid (i.e., a Kalmeyer–Laughlin phase; 126). This has a degree of naturalness as it is easy to conceive of a continuous transition from a d+id SC to a chiral spin liquid. However, it should be mentioned that other studies (123, 124) have found evidence that this intermediate phase is a fully gapped but nonchiral state—which is suggestive that there is a  $\mathbb{Z}_2$  spin liquid (i.e., a Moessner–Sondhi phase; 127) in the 2D limit—or even a gapless spin liquid (125) with a nodal spinon spectrum. Finally, for  $U_{\rm c2} < U$  there is a phase with local correlations corresponding to the 120-deg AF state, known to be the ground state of the 2D model in the large U limit.

**6.1.4.2. Doped cylinders.** The nature of the lightly doped system clearly depends on the character of the undoped parent state. The resulting phase diagram has not nearly been as thoroughly investigated as the case of the square lattice. Particularly interesting is the fate of a lightly doped spin liquid. A spin liquid can be thought of as a quantum disordered SC, such that upon light doping, there is a property inherited from the insulating state, whereas the superfluid stiffness (and hence the ordering temperature) vanishes continuously as  $x \to 0$  (3, 128, 129). Specifically, light doping of a gapped spin liquid could lead to a gapped SC—with the superconducting gap derived from the spin-liquid gap—which is chiral [d + id; (130)] or nonchiral depending on the nature of the spin liquid from which it arose—whereas a nodal spin liquid naturally connects to a nodal SC (131). There is preliminary DMRG evidence that each of these may occur on the triangular lattice under appropriate circumstances (120, 122, 125, 132, 133).

**6.1.5.** The kagome lattice. The Heisenberg model on the kagome lattice is a paradigmatic example of a geometrically frustrated quantum magnet. It has long been suspected that this system does not order magnetically, even with only nearest-neighbor *J*. Different ground states have been proposed based on exact diagonalization of finite clusters (134–139), and various approximate approaches (for a discussion, see 139, 140).

DMRG calculations on cylinders of width up to W=17 have been performed (141–145). (In some of these calculations, a small second-neighbor  $J' \leq 0.15J$  has been applied.) These works consistently find a quantum disordered ground state with no sign of magnetic or valence bond crystalline order. This suggests a QSL ground state. Unfortunately, there is disagreement on the nature of this spin liquid, e.g., whether it has a spin gap (143) or a gapless Dirac spinon spectrum (145). The disagreements suggest that the long-range correlations may not yet be fully converged with respect to the bond dimension, and more extensive studies are needed to resolve the nature of the ground state.

In the studies of the doped system carried out to date (146, 147), light doping of the kagome spin liquid seemingly leads to a holon crystal phase—an insulating state with one doped hole but zero spin per unit cell—rather than to an SC.

#### 6.2. Quantum Monte Carlo Results

The determinant quantum Monte Carlo (DQMC) method (148–151) is a powerful technique to find equilibrium properties of interacting fermions. It is controlled, in the sense that the results are guaranteed to converge to the exact answers upon increasing the computational effort. Unfortunately, in many cases of interest, the applicability of the DQMC method is limited due to the fermion sign problem (152). In these cases, the computational cost for a given accuracy increases exponentially with the system size and the inverse temperature. The repulsive Hubbard model suffers from the fermion sign problem in DQMC at generic values of the filling. Below, we briefly review some useful results that were nevertheless obtained using DQMC, either for special parameters in which the sign problem is absent or by employing very large computational resources to overcome the sign problem.

The U > 0 Hubbard model is sign problem free if the system is particle–hole symmetric (150). This is the case at half-filling (n = 1) on a bipartite lattice (e.g., square or honeycomb) when the intrasublattice hopping is set to zero. Note that the sign of U can be changed by performing a particle–hole transformation on one spin species, showing that the U < 0 Hubbard model is sign problem free with zero total magnetization and an arbitrary filling. The Hubbard model has been simulated using DQMC on a square lattice (150), showing a clear Mott gap and an AF (Néel) ground state for all U > 0.

On the honeycomb lattice, the semimetal state with Dirac nodes is stable for sufficiently small U, whereas the ground state for sufficiently large U is a collinear sublattice antiferromagnet with opposite spin polarization on the two sublattices (153, 154). Initial simulations suggested a QSL state at intermediate U between the semimetal and the antiferromagnet (155); however, the current consensus is that there is a direct continuous transition between the semimetal and AF phases with no intermediate phase (156, 157).

The bilayer Hubbard model has been studied at half-filling for the square (158–160) and honeycomb (56, 161) lattices. In the latter case, motivated by Bernal-stacked bilayer graphene, an AB stacking has been considered. In this case, the noninteracting band structure has quadratic band touchings, and the system may be expected to be unstable even in the presence of arbitrarily weak U, as discussed in Section 5.1. However, it was found that for weak interactions, the dispersion gets renormalized, and each quadratic band touchings splits into four linearly dispersing Dirac

points (56). As a result, a finite U is needed to bring the system from the semimetal into the AF phase, much as in the single-layer honeycomb model.

Finally, DQMC has been applied to the square (102, 162–164) and honeycomb (165) lattice away from half-filling. These calculations require massive computing resources. The square lattice calculations have currently been performed for systems of size L=8 at temperatures down to  $T/t \simeq 0.2$  and interaction strength U/t=8. At these temperatures, finite size effects are found to be small, such that L=8 is probably sufficient to make inferences about the thermodynamic limit. No broken symmetry phase was found. However, there are significant short-range correlations (162) indicative of incommensurate unidirectional SDW, d-wave superconductivity, as well as nematic bond order (164), that grow as the temperature decreases.

#### 7. ARE THERE EXOTIC PHASES IN THE HUBBARD MODEL?

Progress has been made in recent years in constructing reverse engineered model Hamiltonians—such as the Kitaev model or the quantum dimer model—that exhibit exotic quantum phases of various sorts. This is sufficient to settle certain long-standing issues of principle—such as whether QSL phases exist. However, to address whether it is reasonable to expect such phases to arise without extreme fine tuning, it is worthwhile to ask whether these arise in some version of the Hubbard model—with some particular lattice geometry or some range of U/t or t'/t.

#### 7.1. Phases with Exotic Broken Symmetries

Two novel classes of broken symmetry phases have been proposed as candidate orders to account for some observed anomalies in the cuprate high-temperature SCs: states with orbital loop current order (166, 167) and pair-density wave (PDW) states (168–170) with spatially modulated superconducting order.

**7.1.1. Orbital loop current order.** These are states that are close relatives of a CDW, but which break time-reversal symmetry, i.e., in which

$$\left\langle i \sum_{\sigma} \left( c_{j,\sigma}^{\dagger} c_{k,\sigma} - c_{k,\sigma}^{\dagger} c_{j,\sigma} \right) \right\rangle = J_{jk} \neq 0.$$
 34.

Two particularly important such proposals are a zero-momentum intraunit cell orbital antiferromagnet in which  $J_{jk} = J(R_j - R_k)$ , which has ordering vector  $\mathbf{Q} = \mathbf{0}$ , and a d-density wave, in which—on a square lattice in particular— $J_{jk} = e^{i\mathbf{Q}\cdot\mathbf{R}_j}J(R_j - R_k)$  with  $\mathbf{Q} = (\pi,\pi)$ . In both these examples,  $J(\mathbf{R})$  transforms nontrivially under the operations of the point group. Another related state—of which the triplet d-density wave is an example (171)—is a spin-current density wave—which preserves time-reversal symmetry.

As far as we know, convincing evidence for the existence of such phases has not been found in either numerical or controlled approximate studies of Hubbard models. DMRG calculations on doped Hubbard ladders that have probed such order typically have found very weak, extremely short-range current-current correlations (106, 172–174).

There is evidence (discussed in Section 7.2) that a chiral spin-liquid phase arises in a small but finite range of U/t in the undoped Hubbard model on the triangular lattice. Furthermore, for a band structure with a symmetry protected quadratic band-touching, there is a dominant

<sup>&</sup>lt;sup>9</sup>In Reference 173, indications of loop current order were found for relatively large x in a three-band model with substantial nearest-neighbor V, but this was found to arise in an unphysical range of parameters, i.e., one in which the undoped system is not an AFI.

tendency toward an anomalous quantum Hall state at weak coupling (53). Although these states break time-reversal symmetry, they must have a zero-orbital current on any link lying in a mirror plane. However, a CDW state in doped versions of either of these seems likely to support orbital loop current order.

**7.1.2.** Pair-density wave. A PDW is a close relative of the famous Fulde–Ferrell–Larkin–Ovchinniko states (175, 176) that arise (at least in theory) in conventional SCs in response to a small degree of spin polarization. As the name suggests, this is a superconducting state with a pair field that is spatially modulated:

$$\left\langle c_{j,\uparrow}^{\dagger} c_{k,\downarrow} + c_{k,\uparrow}^{\dagger} c_{j,\downarrow} \right\rangle = \Phi(\mathbf{R}_j, \mathbf{R}_k) \neq 0,$$
 35.

where in contrast with any conventional superconducting state, the spatial average of  $\Phi$  vanishes:  $\sum_{R} \Phi(R, R + r) = 0$  for fixed r. (This is a spin-singlet PDW—one can also consider the possibility of a spin-triplet PDW.) Such states have been found as close competitors in certain variational treatments of the Hubbard model, and short-range PDW correlations have been reported in several different DMRG calculations on Hubbard ladders. Furthermore, to date, no clear evidence of PDW long-range order (or even of sufficiently strong quasi-long-range order to lead to a divergent PDW susceptibility) has been presented in studies of any version of the Hubbard model (177, 178), except in one dimension (179, 180). However, the observation of clear PDW short-range order in some cases is a promising point of departure for future investigations (168, 181, 182).

#### 7.2. Phases with Topological Character

There has been an extensive search for spin-liquid phases in Hubbard models with an odd integer number of electrons per unit cell. Here, as discussed in Section 2, it follows from the generalized LSMOH theorem that any insulating phase that preserves translation symmetry must be a topologically ordered spin liquid phase that cannot be adiabatically connected to any band-insulator. At present, though there is no absolutely convincing evidence of such a phase, as discussed in Section 6.1, there are several systems for which DMRG results are highly suggestive of the existence of QSL phases, albeit for relatively narrow ranges of parameters.

#### 8. SPECULATIONS CONCERNING THE PHASE DIAGRAM IN $d \ge 2$

Until this point, we have presented results that are established with some degree of theoretical certainty. Alas, this means we have not been able to present any results for what might a priori be considered the most important regime—spin- $\frac{1}{2}$  fermions with density near but not equal to 1 per site and U comparable to the bandwidth. This is the range of parameters that is likely most relevant to phenomena in a host of highly correlated materials, including the cuprate and various organic SCs. In this final section, we make a speculative attempt to extrapolate from regimes in which our theoretical understanding is solid to obtain a global picture of the phases and regimes of the Hubbard model—particularly focused on the properties of the model in two dimensions.

#### 8.1. The Square Lattice Hubbard Model

In **Figure 5***a*, we show a schematic T = 0 phase diagram in the  $U/t - \mu$  plane of the square lattice Hubbard model with nonvanishing second-neighbor hopping matrix,  $t/t \neq 0$ . On the basis of the weak coupling analysis, we know that for  $U/8t \ll 1$ , there is a uniform *d*-wave SC phase with no other forms of coexisting order. (Here 8*t* is the noninteracting bandwidth.) In the large *U* limit and for a range of doping  $0 < x \leq 0.2$ , one can conclude on the basis of DMRG studies that there

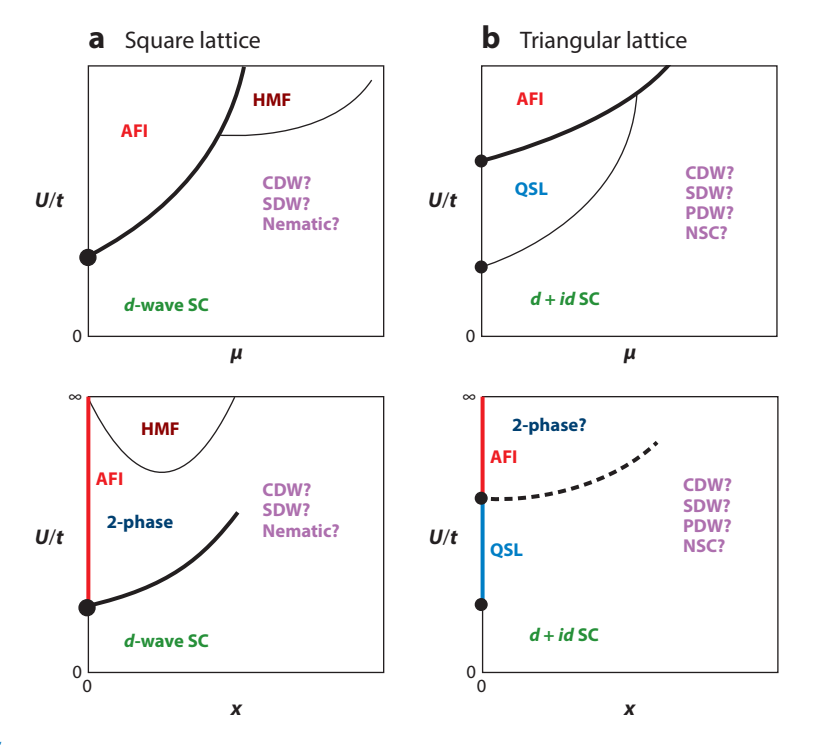


Figure 5

Speculative ground state phase diagrams of the Hubbard model as a function of U and chemical potential,  $\mu$ (upper panels), or doped hole density, x (lower panels). (a) Square lattice with  $t \gg |t'| > 0$ . AFI indicates an insulating (incompressible) phase with Néel antiferromagnetic order and doped hole density x = 0. The thick solid line indicates a first-order transition from the AFI to a compressible phase, and the black circles denote points at which x = 0 in the compressible phase. "2-phase" denotes a region of two-phase coexistence. HMF denotes a half-metallic ferromagnetic phase. At intermediate U/8t, there is clear numerical evidence of multiple local ordering tendencies of comparable strengths including unidirectional CDW, colinear unidirectional SDW, nematic, and d-wave SCs. Which of these phases actually orders is still uncertain. (b) Triangular lattice. At weak coupling, the ground state is a  $d_{x^2-y^2} + id_{xy}$  SC. DMRG studies suggest that for x = 0 as a function of increasing U there is an insulating QSL phase when U is comparable with the bandwidth, 9t, that lies between the small USC and the large U three-sublattice 120-deg-ordered AFI phase. The transition from the OSL to the AFI is likely first order. For  $U \sim 9t$  and finite x, there is DMRG evidence of at least short-range tendencies to d + id and nematic superconducting order, as well as CDW, SDW, and PDW phases. Abbreviations: AFI, antiferromagnetic insulator; CDW, charge-density wave; DMRG, density-matrix-renormalization group; NSC, nematic superconducting; PDW, pair-density wave; QSL, quantum spin liquid; SC, superconductor; SDW, spin-density wave.

is a fully polarized ferromagnetic phase—an HMF. Furthermore, there are compelling theoretical arguments (62, 183) (which we will not review here) that there is a direct first-order transition from the AF insulating phase to the half-metallic ferromagnetic phase, giving rise to the region of two-phase coexistence indicated, with the density of the compressible phase going as  $x_c \sim \sqrt{8t/U}$  as  $U \to \infty$ .

Independent of U, in the dilute electron limit (not shown), the system behaves as a Fermi liquid down to an exponentially low energy scale, below which it presumably forms an unconventional superconducting state by some version of the Kohn–Luttinger mechanism. Finally, for the half-filled band (x = 0) and U/8t greater than a critical value,  $\alpha_c$ , there is an insulating phase that, so

long as  $t'/t \lesssim 1/2$  (so the magnetism is not terribly frustrated), exhibits long-range Néel order (as discussed in Section 5.4.1,  $\alpha_c \sim 1/\ln|t/t'| \to 0$  as  $t'/t \to 0$ ).

In **Figure 5**, we have indicated a presumed direct (and consequently first order) transition from the *d*-wave SC at x=0 to the insulating AF phase. Such a direct transition occurs in HF approximation (or equivalently in a suitable large N limit) for small t/t, although at larger t/t there can arise an intermediate AF metal (i.e., only partially gapped) phase (S. Raghu, unpublished manuscript). Assuming the transition at x=0 is first order, the transition must remain first order for a range of chemical potentials. Consequently, for small  $U/8t > \alpha_c$  there must exist a two-phase coexistence region corresponding to the thick solid line in the figure.

Indeed, arguments suggesting that the AF insulating phase is generically bounded by a line of first-order transitions (leading to phase separation) were summarized in Reference 76, and more recently these arguments have been supported by extensive variational Monte Carlo studies of the Hubbard model in Reference 184. Another candidate small x phase when  $U/8t \gtrsim \alpha_c$  that is suggested by HF studies (77–79) (especially in the limit t'=0) is an insulating incommensurate unidirectional colinear SDW (stripe) phase. The stripe phase can be thought of as a form of microphase separation.

Unfortunately, the structure of the middle part of the phase diagram, where  $U/8t \sim 1$  and  $1/12 \lesssim x \lesssim 1/3$ , is presently unsettled. From DMRG and other studies, it is clear that there are strong local tendencies toward *d*-wave SCs, as well as unidirectional (stripe) CDW and SDW orders. Implicit in the observation of striped states is a strong tendency toward lattice rotational symmetry breaking, i.e., nematic order.<sup>10</sup>

That all DMRG studies (as well as other less controlled methods) find strong local tendencies toward a *d*-wave SC is compatible with the supposition that the Hubbard model at intermediate coupling captures an essential feature of cuprate physics that leads to high-temperature *d*-wave SCs. However, whether the Hubbard model has more than a *d*-wave tendency—i.e., whether it actually supports a robust *d*-wave SC phase at intermediate *U* or not—is still unsettled. Under most circumstances, especially in broader ladders, the DMRG studies suggest that the competing tendency toward CDW order may be stronger.

#### 8.2. The Triangular Lattice Hubbard Model

Figure 5*b* shows a conjectured phase diagram for the triangular lattice Hubbard model. Again, from a weak coupling analysis, we know that the small *U* portion of the phase diagram is superconducting, likely a d + id SC (185, 186). At n = 1 and large enough *U*, the model is equivalent to a spin- $\frac{1}{2}$  Heisenberg model, for which strong evidence exists that the ground state has long-range, coplanar three sublattice insulating AF order—the 120-deg state. DMRG studies consistently indicate the existence of an intermediate insulating phase without any long or quasi-long-range AF order—corresponding to some sort of QSL. Thus, at x = 0 there are two transitions as a function of U/8t. The exact nature of the QSL, however, is still controversial.

There is some evidence that the QSL in question is a chiral spin liquid, which would be compatible with a continuous transition to a chiral (d + id) SC upon light doping, as shown in the figure. Then at larger doping and intermediate values of U/8t, there is evidence from DMRG studies of a local tendency toward a variety of possible broken symmetry phases including SDW, CDW, PDW, and NSC. However, again, which of these orders exist as ground state phases in

<sup>&</sup>lt;sup>10</sup>This interpretation requires some care because of the effects of the boundaries, which are present in most DMRG calculations.

two dimensions is still an open question. Preliminary evidence (120) that the SC tendencies are particularly strong at small x and for U in the spin-liquid regime offers some encouragement for the long cherished ideal that a spin liquid may be a high-temperature SC waiting to happen.

#### 9. IMPORTANT OPEN QUESTIONS

We end by highlighting some of the major outstanding challenges in the physics of the Hubbard model. We discuss whether the Hubbard model exhibits high-temperature superconductivity and/or other exotic phases.

#### 9.1. Is the Hubbard Model a High-Temperature Superconductor?

It has been established that the repulsive U Hubbard model has a superconducting ground state at small U, but it still remains uncertain whether—and if so under what circumstances—it supports high-temperature superconductivity. In other words, are there circumstances (i.e., some range of band structure parameters) in which the Hubbard model is superconducting when all the energy scales are comparable, i.e., when U is on the order of the bandwidth, so that  $T_{\rm c}$ —if a SC state arises—is a sizable fraction of  $E_{\rm F}$ ? To get a quantitative feeling, recall that the bandwidth in the cuprates is of the order of  $W \sim 2$  eV. Taking  $W \simeq 8t$ , we obtain that a  $T_{\rm c}$  of 0.05t would correspond to  $T_{\rm c} \sim 150$  K, which is of the order of the maximal transition temperature found in the cuprates. Although affirmative answers to this question have been suggested on the basis of various approximate calculations, the presence of multiple intertwined orders—with the consequent existence of subtle energies that are difficult to capture reliably—renders the validity of these approximate results uncertain.

#### 9.2. What Exotic Phases Arise?

At the same time, though there are various reasons to feel that exotic forms of quantum order can arise in the Hubbard model—at least if the underlying band structure cooperates—currently the evidence for these states ranges from suggestive to absent. Ideally, one would like to identify versions of the model that unambiguously exhibit various forms of insulating QSLs, PDW SCs (in more than one dimension), and/or possible forms of orbital loop current order.

#### 9.3. What Sort of Non-Fermi-Liquid Behaviors Occur at Elevated T?

We have hardly touched on the nature of the model at finite T (although much is known) and have totally neglected any issues associated with near equilibrium dynamical properties, much less the far from equilibrium behaviors that are of so much recent interest. For instance, for U on the order of the bandwidth, there most probably will not be a broad range of T above all ordering temperatures in which the system can be well described by the weakly interacting quasi particles of Fermi liquid theory. What the behavior is in this regime of T—especially including what processes govern the dissipative linear response of the system—is one of the most important open areas in the field.

#### 9.4. Have We Learned Anything Useful?

Finally, we have discussed controlled solutions of the Hubbard model—and have emphasized the limited progress that has been made even on this simplest of all model strongly correlated systems. Obviously, from a broader perspective, much simpler and more versatile methods of solution

[2 (in this volume), 187, 188] are needed that, once benchmarked by comparison with the controlled results discussed here, can be applied more widely and perhaps even in ways that interface with microscopic electronic structure approaches (189–191).

#### **DISCLOSURE STATEMENT**

The authors are not aware of any affiliations, memberships, funding, or financial holdings that might be perceived as affecting the objectivity of this review.

#### **ACKNOWLEDGMENTS**

It is a pleasure to acknowledge numerous extremely helpful discussions about the Hubbard model and related topics with too many colleagues to list. In particular, however, the writing of this paper was greatly assisted by input from Ian Affleck, Assa Auerbach, Vladimir Calvera, Andrey Chubukov, Youjin Deng, Tom Devereaux, Eduardo Fradkin, Zhaoyu Han, Hong-Chen Jiang, Elliott Lieb, Dror Orgad, Mohit Randeria, Doug Scalapino, and Richard Scalettar. S.A.K. was supported, in part, by the National Science Foundation (NSF) under grant number DMR2000987. E.B. acknowledges support from the European Research Council (ERC) under grant HQMAT (grant agreement number 817799). S.R. was supported in part by the Department of Energy, Office of Basic Energy Sciences, Division of Materials Sciences and Engineering, under contract DE-AC02-76SF00515.

#### LITERATURE CITED

- 1. Hubbard J. 1963. Proc. R. Soc. Lond. Ser. A Math. Phys. Sci. 276(1365):238-57
- 2. Qin M, Schäfer T, Andergassen S, Corboz P, Gull E. 2022. Annu. Rev. Condens. Matter Phys. 13:275–302
- 3. Anderson PW. 1987. Science 235(4793):1196-98
- 4. Emery VJ. 1987. Phys. Rev. Lett. 58(26):2794-97
- 5. Scalapino DJ. 2012. Rev. Mod. Phys. 84(4):1383-417
- 6. Lieb EH, Loss M, McCann RJ. 1993. J. Math. Phys. 34(3):891-98
- 7. Yang CN. 1989. Phys. Rev. Lett. 63(19):2144-47
- 8. Zhang S. 1991. Int. 7. Mod. Phys. B 5(1):153-67
- 9. Yang CN, Zhang SC. 1990. Mod. Phys. Lett. B 04(11):759-66
- 10. Lieb EH. 1989. Phys. Rev. Lett. 62(10):1201-4
- 11. Lieb E, Mattis D. 1962. 7. Math. Phys. 3(4):749-51
- 12. Tasaki H. 1989. Phys. Rev. B 40(13):9192-93
- 13. Tasaki H. 2021. Physics and Mathematics of Quantum Many-Body Systems. Cham, Switz.: Springer
- 14. Nagaoka Y. 1966. Phys. Rev. 147(1):392-405
- 15. Thouless DJ. 1965. Proc. Phys. Soc. 86(5):893–904
- 16. Lieb E, Schultz T, Mattis D. 1961. Ann. Phys. 16(3):407-66
- 17. Yamanaka M, Oshikawa M, Affleck I. 1997. Phys. Rev. Lett. 79(6):1110-13
- Oshikawa M. 2000. Phys. Rev. Lett. 84(7):1535–38
- 19. Hastings MB. 2004. Phys. Rev. B 69(10):104431
- 20. Laughlin RB. 1981. Phys. Rev. B 23(10):5632-33
- 21. Parameswaran SA, Turner AM, Arovas DP, Vishwanath A. 2013. Nat. Phys. 9(5):299-303
- 22. Watanabe H, Po HC, Vishwanath A, Zaletel M. 2015. PNAS 112(47):14551-56
- 23. Schumann R. 2002. Ann. Phys. 11(1):49-87
- 24. Scalapino DJ, Trugman SA. 1996. Philos. Mag. B 74(5):607-10
- 25. Yao H, Kivelson SA. 2010. Phys. Rev. Lett. 105(16):166402
- 26. White SR, Chakravarty S, Gelfand MP, Kivelson SA. 1992. Phys. Rev. B 45(9):5062-65
- 27. Altman E, Auerbach A. 2002. Phys. Rev. B 65(10):104508

- 28. Tsai WF, Kivelson SA. 2006. Phys. Rev. B 73(21):214510. Erratum. 2007. Phys. Rev. B 76:139902
- 29. Yao H, Tsai WF, Kivelson SA. 2007. Phys. Rev. B 76(16):161104
- 30. Baruch S, Orgad D. 2010. Phys. Rev. B 82(13):134537
- 31. Wachtel G, Baruch S, Orgad D. 2017. Phys. Rev. B 96(6):064527
- 32. Ying T, Mondaini R, Sun XD, Paiva T, Fye RM, Scalettar RT. 2014. Phys. Rev. B 90(7):075121
- 33. Karakonstantakis G, Berg E, White SR, Kivelson SA. 2011. Phys. Rev. B 83(5):054508
- 34. Lieb EH, Wu FY. 1968. Phys. Rev. Lett. 20(25):1445-48
- 35. Lin HH, Balents L, Fisher MPA. 1997. Phys. Rev. B 56(11):6569-93
- Emery VJ, Kivelson SA, Zachar O. 1997. Phys. Rev. B 56(10):6120–47
- 37. Giamarchi T. 2003. Quantum Physics in One Dimension, Vol. 121. Oxford, UK: Clarendon Press
- 38. Kohn W, Luttinger JM. 1965. Phys. Rev. Lett. 15(12):524-26
- 39. Scalapino DJ, Loh E, Hirsch JE. 1986. Phys. Rev. B 34(11):8190-92
- 40. Bealmonod M, Bourbonnais C, Emery V. 1986. Phys. Rev. B 34(11):7716–20
- 41. Maiti S, Chubukov AV. 2013. AIP Conf. Proc. 1550(1):3-73
- Polchinski J. 1993. In Theoretical Advanced Study Institute in Elementary-Particle Physics: Recent Directions in Particle Theory: From Superstrings and Blackholes to the Standard Model (TASI '92), pp. 235–74. Singapore: World Sci.
- 43. Shankar R. 1994. Rev. Mod. Phys. 66(1):129-92
- 44. Kagan MY, Chubukov AV. 1988. Sov. 7. Exp. Theor. Phys. Lett. 47:614-17
- 45. Raghu S, Kivelson SA, Scalapino DJ. 2010. Phys. Rev. B 81(22):224505
- 46. Hlubina R. 1999. Phys. Rev. B 59(14):9600-5
- 47. Deng Y, Kozik E, Prokof'ev NV, Svistunov BV. 2015. Europhys. Lett. 110(5):57001
- 48. Markiewicz RS. 1997. J. Phys. Chem. Solids 58(8):1179-310
- 49. Dzyaloshinskii IE. 1987. J. Exp. Theor. Phys. 66(4):848-54
- 50. Schulz HJ. 1987. Europhys. Lett. 4(5):609-15
- 51. Abrikosov AA, Beneslavskii SD. 1971. J. Low Temp. Phys. 5(2):141-54
- 52. Abrikosov AA. 1974. 7. Exp. Theor. Phys 66:1443-60
- 53. Sun K, Yao H, Fradkin E, Kivelson SA. 2009. Phys. Rev. Lett. 103(4):046811
- 54. Vafek O, Yang K. 2010. Phys. Rev. B 81(4):041401
- 55. Balents L, Fisher MPA. 1996. Phys. Rev. B 53(18):12133-41
- 56. Pujari S, Lang TC, Murthy G, Kaul RK. 2016. Phys. Rev. Lett. 117(8):086404
- 57. Chubukov AV. 2009. Phys. C Supercond. 469(9):640–50
- 58. Ulmke M. 1998. Eur. Phys. 7. B Condens. Matter Complex Syst. 1(3):301-4
- 59. Mielke A. 1991. 7. Phys. A Math. Gen. 24(2):L73-77
- 60. Mielke A. 1992. J. Phys. A Math. Gen. 25(16):4335-45
- 61. Shastry BS, Krishnamurthy HR, Anderson PW. 1990. Phys. Rev. B 41(4):2375-79
- 62. Emery VJ, Kivelson SA, Lin HQ. 1990. Phys. Rev. Lett. 64(4):475-78
- 63. Liu L, Yao H, Berg E, White SR, Kivelson SA. 2012. Phys. Rev. Lett. 108(12):126406
- 64. Abrikosov AA, Khalatnikov IM. 1958. Sov. Phys. J. Exp. Theor. Phys. 6(5):888–92
- 65. Engelbrecht JR, Randeria M, Zhang L. 1992. Phys. Rev. B 45(17):10135-38
- 66. Galitskii VM. 1958. Sov. Phys. 7. Exp. Theor. Phys. 7(1):104-12
- 67. Chubukov AV. 1993. Phys. Rev. B 48(2):1097-104
- 68. Affleck I, Marston JB. 1988. *Phys. Rev. B* 37(7):3774–77
- 69. Arovas DP, Auerbach A. 1988. Phys. Rev. B 38(1):316-32
- 70. Marston JB, Affleck I. 1989. Phys. Rev. B 39(16):11538-58
- 71. Read N, Sachdev S. 1991. Phys. Rev. Lett. 66(13):1773-76
- 72. Hewson AC. 1993. In Cambridge Studies in Magnetism. Cambridge, UK: Cambridge Univ. Press
- 73. Auerbach A. 1994. Interacting Electrons and Quantum Magnetism. New York: Springer-Verlag
- Fradkin E. 2013. Field Theories of Condensed Matter Physics. Cambridge, UK: Cambridge Univ. Press. 2nd ed.
- 75. Schulz HJ. 1995. 7. Low Temp. Phys. 99(3):615-24

- Kivelson SA, Emery VJ. 1994. In Strongly Correlated Electronic Materials, Proceedings of The Los Alamos Symposium, 1993, ed. KS Bedell, Z Wang, DE Meltzer, AV Balatsky, E Abrahams, pp. 619–56. Redding, MA: Addison-Wesley
- 77. Zaanen J, Gunnarsson O. 1989. Phys. Rev. B 40(10):7391–94
- 78. Schulz HJ. 1989. J. Phys. France 50(18):2833-49
- 79. Machida K. 1989. Phys. C Supercond. 158(1):192-96
- 80. Schulz HJ. 1990. Phys. Rev. Lett. 64(12):1445-48
- 81. White SR. 1992. Phys. Rev. Lett. 69(19):2863-66
- 82. Schollwöck U. 2011. Ann. Phys. 326(1):96-192
- 83. Ostlund S, Rommer S. 1995. Phys. Rev. Lett. 75(19):3537-40
- 84. Dolfi M, Bauer B, Keller S, Troyer M. 2015. Phys. Rev. B 92(19):195139
- 85. Verstraete F, Wolf M, Pérez-García D, Cirac JI. 2006. Int. J. Mod. Phys. B 20(30n31):5142-53
- 86. White SR, Feiguin AE. 2004. Phys. Rev. Lett. 93(7):076401
- 87. Yang C, Feiguin AE. 2019. Phys. Rev. B 99(23):235117
- 88. Haldane FDM. 1983. Phys. Lett. A 93(9):464-68
- 89. Chakravarty S. 1996. Phys. Rev. Lett. 77(21):4446-49
- 90. Jiang HC, Yao H, Balents L. 2012. Phys. Rev. B 86(2):024424
- 91. Figueirido F, Karlhede A, Kivelson S, Sondhi S, Rocek M, Rokhsar DS. 1990. Phys. Rev. B 41(7):4619-32
- 92. Gong SS, Zhu W, Sheng DN, Motrunich OI, Fisher MPA. 2014. Phys. Rev. Lett. 113(2):027201
- 93. Noack RM, White SR, Scalapino DJ. 1995. Europhys. Lett. 30(3):163-68
- 94. Troyer M, Tsunetsugu H, Rice TM. 1996. Phys. Rev. B 53(1):251-67
- 95. Poilblanc D, Chiappa O, Riera J, White SR, Scalapino DJ. 2000. Phys. Rev. B 62(22):R14633-36
- 96. Gannot Y, Jiang YF, Kivelson SA. 2020. Phys. Rev. B 102(11):115136
- 97. Luther A, Emery VJ. 1974. Phys. Rev. Lett. 33(10):589-92
- 98. White SR, Affleck I, Scalapino DJ. 2002. Phys. Rev. B 65(16):165122
- 99. Schulz HJ. 1980. Phys. Rev. B 22(11):5274-77
- 100. White SR, Scalapino DJ. 1997. Phys. Rev. B 55(22):14701-4
- 101. White SR, Scalapino DJ. 1999. Phys. Rev. B 60(2):R753-56
- 102. Huang EW, Mendl CB, Jiang HC, Moritz B, Devereaux TP. 2018. NP7 Quantum Mater. 3:22
- 103. Jiang HC, Devereaux TP. 2019. Science 365(6460):1424-28
- 104. Jiang HC, Weng ZY, Kivelson SA. 2018. Phys. Rev. B 98(14):140505
- 105. Chung CM, Qin M, Zhang S, Schollwöck U, White SR. 2020. Phys. Rev. B 102(4):041106
- 106. Dodaro JF, Jiang HC, Kivelson SA. 2017. Phys. Rev. B 95(15):155116
- 107. Zheng BX, Chung CM, Corboz P, Ehlers G, Qin MP, et al. 2017. Science 358(6367):1155-60
- 108. Jiang YF, Zaanen J, Devereaux TP, Jiang HC. 2020. Phys. Rev. Res. 2(3):033073
- 109. Hager G, Wellein G, Jeckelmann E, Fehske H. 2005. Phys. Rev. B 71(7):075108
- 110. White SR, Scalapino DJ. 2003. Phys. Rev. Lett. 91(13):136403
- 111. Jiang HC, Kivelson SA. 2021. Phys. Rev. Lett. 127:097002
- 112. Gong S, Zhu W, Sheng DN. 2021. Phys. Rev. Lett. 127:097003
- 113. Jiang S, Scalapino DJ, White SR. 2021. arXiv:2104.10149
- 114. Jiang HC, Kivelson SA. 2021. arXiv:2105.07048
- 115. Gong SS, Sheng DN, Motrunich OI, Fisher MPA. 2013. Phys. Rev. B 88(16):165138
- 116. Gong SS, Zhu W, Sheng DN. 2015. Phys. Rev. B 92(19):195110
- 117. Jiang S, Mesaros A, Ran Y. 2014. Phys. Rev. X 4(3):031040
- 118. Yang X, Zheng H, Qin M. 2021. Phys. Rev. B 103(15):155110
- 119. Qin M. 2021. arXiv e-prints arXiv:2104.14160
- 120. Jiang HC. 2021. NPJ Quantum Mater. 6:71
- 121. Szasz A, Motruk J, Zaletel MP, Moore JE. 2020. Phys. Rev. X 10(2):021042
- 122. Zhu Z, Sheng DN, Vishwanath A. 2020. arXiv:2007.11963
- 123. Gong SS, Zhu W, Sheng DN. 2014. Sci. Rep. 4:6317
- 124. Gong SS, Zheng W, Lee M, Lu YM, Sheng DN. 2019. Phys. Rev. B 100(24):241111
- 125. Hu S, Zhu W, Eggert S, He YC. 2019. Phys. Rev. Lett. 123(20):207203

- 126. Kalmeyer V, Laughlin RB. 1987. Phys. Rev. Lett. 59(18):2095–98
- 127. Moessner R, Sondhi SL. 2001. Phys. Rev. Lett. 86(9):1881-84
- 128. Rokhsar DS, Kivelson SA. 1988. Phys. Rev. Lett. 61(20):2376–79
- 129. Laughlin RB. 1988. Science 242:525-33
- 130. Rokhsar DS. 1993. Phys. Rev. Lett. 70(4):493-96
- 131. Balents L, Fisher MPA, Nayak C. 1998. Int. J. Mod. Phys. B 12(10):1033-68
- 132. Jiang YF, Jiang HC. 2020. Phys. Rev. Lett. 125(15):157002
- 133. Venderley J, Kim EA. 2019. Phys. Rev. B 100(6):060506
- 134. Zeng C, Elser V. 1990. Phys. Rev. B 42(13):8436-44
- 135. Chalker JT, Eastmond JFG. 1992. Phys. Rev. B 46(21):14201-4
- 136. Lecheminant P, Bernu B, Lhuillier C, Pierre L, Sindzingre P. 1997. Phys. Rev. B 56(5):2521-29
- 137. Läuchli AM, Sudan J, Sørensen ES. 2011. Phys. Rev. B 83(21):212401
- 138. Nakano H, Sakai T. 2011. J. Phys. Soc. Jpn. 80(5):053704
- 139. Läuchli AM, Sudan J, Moessner R. 2019. Phys. Rev. B 100(15):155142
- 140. Changlani HJ, Kochkov D, Kumar K, Clark BK, Fradkin E. 2018. Phys. Rev. Lett. 120(11):117202
- 141. Yan S, Huse DA, White SR. 2011. Science 332(6034):1173-76
- 142. Jiang HC, Weng ZY, Sheng DN. 2008. Phys. Rev. Lett. 101(11):117203
- 143. Jiang HC, Wang Z, Balents L. 2012. Nat. Phys. 8(12):902-5
- 144. Depenbrock S, McCulloch IP, Schollwöck U. 2012. Phys. Rev. Lett. 109(6):067201
- 145. He YC, Zaletel MP, Oshikawa M, Pollmann F. 2017. Phys. Rev. X 7(3):031020
- 146. Jiang HC, Devereaux T, Kivelson SA. 2017. Phys. Rev. Lett. 119(6):067002
- 147. Peng C, Jiang YF, Sheng DN, Jiang HC. 2021. Adv. Quantum Technol. 4(3):2000126
- 148. Blankenbecler R, Scalapino DJ, Sugar RL. 1981. Phys. Rev. D 24(8):2278-86
- 149. Hirsch JE. 1983. Phys. Rev. B 28(7):4059-61
- White SR, Scalapino DJ, Sugar RL, Loh EY, Gubernatis JE, Scalettar RT. 1989. Phys. Rev. B 40(1):506–
   16
- Assaad FF. 2002. In Quantum Simulations of Complex Many-Body Systems: From Theory to Algorithms, Vol. 10, NIC Ser., ed. J Grotendorst, D Marx, A Muyramatsu, pp. 99–156. Jülich, Ger.: Neumann Inst. Comput.
- 152. White SR, Scalapino DJ, Sugar RL, Bickers NE, Scalettar RT. 1989. Phys. Rev. B 39(1):839-42
- 153. Sorella S, Tosatti E. 1992. Europhys. Lett. 19(8):699-702
- 154. Paiva T, Scalettar RT, Zheng W, Singh RRP, Oitmaa J. 2005. Phys. Rev. B 72(8):085123
- 155. Meng ZY, Lang TC, Wessel S, Assaad FF, Muramatsu A. 2010. Nature 464(7290):847-51
- 156. Sorella S, Otsuka Y, Yunoki S. 2012. Sci. Rep. 2(1):1-5
- 157. Assaad FF, Herbut IF. 2013. Phys. Rev. X 3(3):031010
- 158. Bulut N, Scalapino DJ, Scalettar RT. 1992. Phys. Rev. B 45(10):5577-84
- 159. Scalettar RT, Cannon JW, Scalapino DJ, Sugar RL. 1994. Phys. Rev. B 50(18):13419–27
- 160. Bouadim K, Batrouni GG, Hébert F, Scalettar RT. 2008. Phys. Rev. B 77(14):144527
- 161. Lang TC, Meng ZY, Scherer MM, Uebelacker S, Assaad FF, et al. 2012. Phys. Rev. Lett. 109(12):126402
- 162. Huang EW, Mendl CB, Liu S, Johnston S, Jiang HC, et al. 2017. Science 358(6367):1161-64
- 163. Huang EW, Sheppard R, Moritz B, Devereaux TP. 2019. Science 366(6468):987–90
- 164. Liu T, Jost D, Moritz B, Huang EW, Hackl R, Devereaux TP. 2021. Phys. Rev. B 103:134502
- 165. Zhu X, Ying T, Guo H, Feng S. 2019. Chin. Phys. B 28(7):077401
- 166. Varma CM. 1999. Phys. Rev. Lett. 83(17):3538-41
- 167. Chakravarty S, Laughlin RB, Morr DK, Nayak C. 2001. Phys. Rev. B 63(9):094503
- 168. Himeda A, Kato T, Ogata M. 2002. Phys. Rev. Lett. 88(11):117001
- 169. Berg E, Fradkin E, Kim EA, Kivelson SA, Oganesyan V, et al. 2007. Phys. Rev. Lett. 99(12):127003
- Agterberg DF, Davis JS, Edkins SD, Fradkin E, Van Harlingen DJ, et al. 2020. Annu. Rev. Condens. Matter Phys. 11:231–70
- 171. Hsu CH, Wang Z, Chakravarty S. 2012. Phys. Rev. B 86(21):214510
- 172. Scalapino DJ, White SR, Affleck I. 2001. *Phys. Rev. B* 64(10):100506(R)
- 173. Nishimoto S, Jeckelmann E, Scalapino DJ. 2009. Phys. Rev. B 79(20):205115

178. Presents results of a large body of the most recent and unpublished DQMC results on the square lattice Hubbard model

- 174. Kung YF, Chen CC, Moritz B, Johnston S, Thomale R, Devereaux TP. 2014. Phys. Rev. B 90(22):224507
- 175. Fulde P, Ferrell RA. 1964. Phys. Rev. 135(3A):A550-63
- 176. Larkin AI, Ovchinnikov YN. 1964. Zh. Eksp. Teor. Fiz. 47:1136-46
- 177. White SR, Scalapino DJ. 2009. Phys. Rev. B 79(22):220504
- 178. Devereaux TP. 2021. Numerical investigations of models of the cuprates (Harvard CMSC Colloquium). https://www.youtube.com/watch?v=mAYnLdi3vs4
- 179. Berg E, Fradkin E, Kivelson SA. 2010. Phys. Rev. Lett. 105(14):146403
- 180. Jaefari A, Fradkin E. 2012. Phys. Rev. B 85(3):035104
- 181. Corboz P, Rice TM, Troyer M. 2014. Phys. Rev. Lett. 113(4):046402
- 182. Xu XY, Law KT, Lee PA. 2019. Phys. Rev. Lett. 122(16):167001
- 183. Eisenberg E, Berkovits R, Huse DA, Altshuler BL. 2002. Phys. Rev. B 65(13):134437
- 184. Sorella S. 2021. arXiv:2101.07045
- 185. Nandkishore R, Levitov LS, Chubukov AV. 2012. Nat. Phys. 8(2):158-63
- 186. Nandkishore R, Thomale R, Chubukov AV. 2014. Phys. Rev. B 89(14):144501
- 187. Georges A, Kotliar G, Krauth W, Rozenberg MJ. 1996. Rev. Mod. Phys. 68(1):13-125
- 188. LeBlanc JPF, Antipov AE, Becca F, Bulik IW, Chan GKL, et al. 2015. Phys. Rev. X 5(4):041041
- 189. Kent PRC, Kotliar G. 2018. Science 361(6400):348-54
- 190. Paul A, Birol T. 2019. Annu. Rev. Mater. Res. 49:31-52
- 191. Maier T, Jarrell M, Pruschke T, Hettler M. 2005. Rev. Mod. Phys. 77(3):1027-80



### Contents

#### Annual Review of Condensed Matter Physics

Volume 13, 2022

Reflections on 65 Years of Helium Research  John D. Reppy	1
My Life and Science  Valery L. Pokrovsky	15
Russell Donnelly and His Leaks  J.J. Niemela and K.R. Sreenivasan	33
Director Deformations, Geometric Frustration, and Modulated Phases in Liquid Crystals  **Jonathan V. Selinger**	49
Thin Film Skyrmionics  Takaaki Dohi, Robert M. Reeve, and Mathias Kläui	73
The Physics of Dense Suspensions  Christopher Ness, Ryohei Seto, and Romain Mari	97
Topological Magnets: Functions Based on Berry Phase and Multipoles  Satoru Nakatsuji and Ryotaro Arita	119
Active Turbulence Ricard Alert, Jaume Casademunt, and Jean-François Joanny	143
Topological Magnons: A Review  Paul A. McClarty	171
Olfactory Sensing and Navigation in Turbulent Environments  Gautam Reddy, Venkatesh N. Murthy, and Massimo Vergassola	191
Irreversibility and Biased Ensembles in Active Matter: Insights from Stochastic Thermodynamics Étienne Fodor, Robert L. Jack, and Michael E. Cates	215
The Hubbard Model  Daniel P. Arovas, Erez Berg, Steven A. Kivelson, and Srinivas Raghu	239
The Hubbard Model: A Computational Perspective  Mingpu Qin, Thomas Schäfer, Sabine Andergassen, Philippe Corboz,	275
and Emanuel Gull	4/3

Understanding Hydrophobic Effects: Insights from Water Density Fluctuations Nicholas B. Rego and Amish J. Patel	303
Modeling of Ferroelectric Oxide Perovskites: From First to Second Principles  Philippe Ghosez and Javier Junquera	325
How Cross-Link Numbers Shape the Large-Scale Physics of Cytoskeletal Materials  Sebastian Fürthauer and Michael J. Shelley	365
Studying Quantum Materials with Scanning SQUID Microscopy  Eylon Persky, Ilya Sochnikov, and Beena Kalisky	385
Coherently Coupled Mixtures of Ultracold Atomic Gases  Alessio Recati and Sandro Stringari	407

#### Errata

An online log of corrections to *Annual Review of Condensed Matter Physics* articles may be found at http://www.annualreviews.org/errata/conmatphys